DESIGN OF HIGH FREQUENCY VOLTAGE-CONTROLLED PULSE OSCILLATOR

by

KARL B. KEHLER

SUBMITTED IN PARTIAL FULFILLMENT OF THE REQUIREMENTS FOR THE DEGREE OF MASTER OF SCIENCE at the MASSACHUSETTS INSTITUTE OF TECHNOLOGY

June, 1966

Signature of the Author___
Department of Electrical Engineering, May 20, 1966

Certified by_____
Thesis Supervisor

Accepted by_____
Chairman, Departmental Committee on Graduate Students

DESIGN OF HIGH FREQUENCY VOLTAGE-CONTROLLED PULSE OSCILLATOR

by

KARL BUCK KEHLER

Submitted to the Department of Electrical Engineering on May 20, 1966, in partial fulfillment of the requirements for the degree of Master of Science.

In this thesis the analysis and design of a linear voltage-controlled pulse oscillator is discussed. The output of this device is a frequency which is proportional to the input d-c control voltage. Measurements of the oscillator performance are compared with a theoretical analysis based on a model of the circuit with the conclusion that the model used is an accurate representation of the actual circuit.

An averaging feedback technique was employed to realize the linear transfer function which is 10^7 MHz/volt to an accuracy of $\pm$ 1%. The output covers the decade of frequency from 5.0 to 50 MHz which corresponds to a d-c control voltage ranging from 0.5 to 5.0 volts.

Thesis Supervisor: Bruce Daniels Wedlock, Sc.D.

Title: Assistant Professor of Electrical Engineering

The author would like to express gratitude to the General Radio Company for allowing the research for this thesis to be performed at the Company's engineering offices.

Special thanks are also extended to James K. Skilling, Development Engineer at the General Radio Company, for his advice in design problems and to Professor Bruce D. Wedlock for supervising the work and editing the manuscript.

Karl B. Kehler

May 20, 1966

TABLE OF CONTENTS

LIST OF FIGURES

1.0 INTRODUCTION

1.1 Statement of Problem

This thesis describes the design of a voltage controlled pulse oscillator (VCPO). The frequency of the output is porportional to the d-c level of the control voltage. Frequency in the range 5 to 50 MHz is covered which corresponds to control voltage in the interval 0.5 to 5.0 volts.

The design objective was to provide one decade of frequency with a linear transfer function (control voltage to frequency) that is accurate to 1%; and the highest output frequency was to be at least 30 MHz.

1.2 Other Work in the Area

There are several ways of building a VCPO whose output frequency is proportional to control voltage. Most of these methods are unsuitable for operation at the high frequencies required in this thesis. In the sections that follow, three different methods for building linear VCPO's will be discussed and their limitations at high frequency will be pointed out.

1.21 A schematic diagram that demonstrates ramp timing is shown in Figure 1. During the charging interval the switch is in position S_c allowing C_T to be charged by the constant current source I_c. The switch changes to position S_D when V_T reaches the reference voltage E_c so C_T is discharged by a constant current I_D. The switch changes position and the cycle repeats when V_T decays to the reference voltage E_D.

The period for the ramp timing circuit of Figure 1 is given in Equation 1 as the sum of the charging and discharging times.

$$T = T_c + T_D$$

$$= \frac{C_T (E_c - E_D)}{I_c} + \frac{C_T (E_c - E_D)}{I_D} \qquad (1)$$

If I_c is much larger than I_D the charging time can be neglected with respect to the discharge time in Equation 1 and the frequency becomes:

$$f = 1/T \approx I_D/C_T(E_c - E_D) \qquad (2)$$

The frequency given in Equation 2 is proportional to I_D which is the desired transfer function if I_D is a voltage controlled current source.

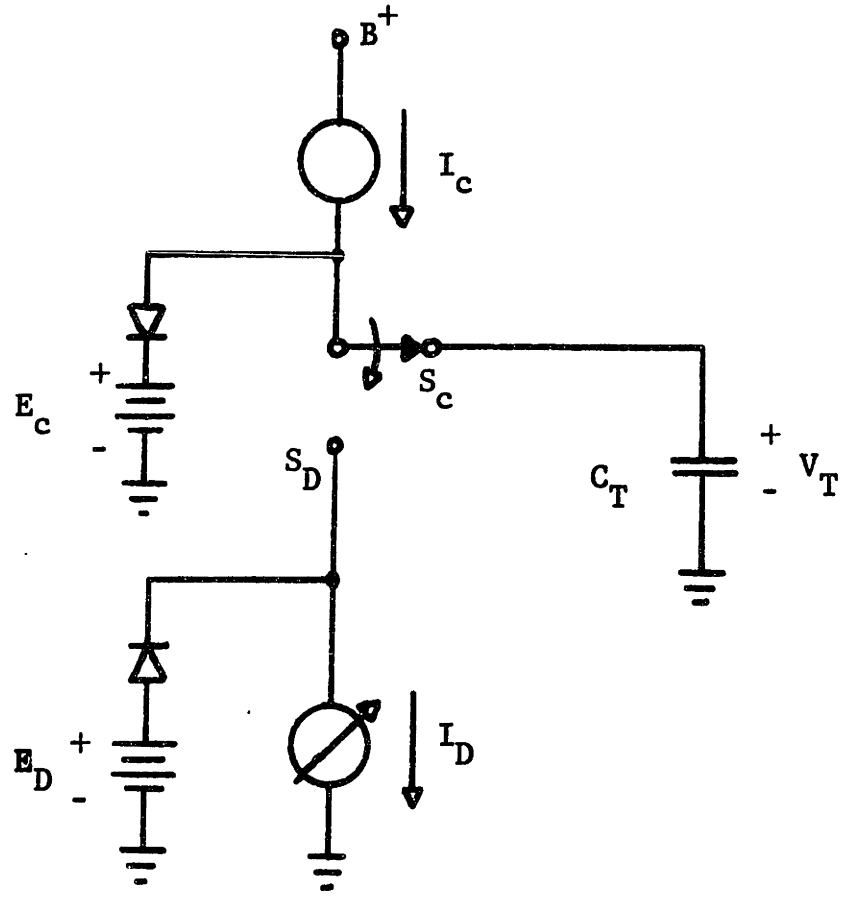

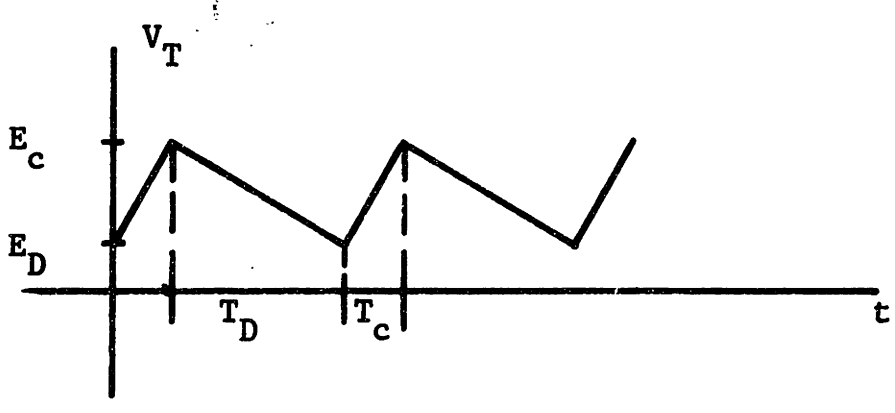

RAMP TIMING

FIGURE 1

At high frequency the charging time cannot be neglected due to limitations on the size of I_c, I_D, and C_T; with the result that the frequency is no longer proportional to control voltage.

See References 1 and 2 for circuit descriptions of VCPO's using ramp timing.

1.22 Emitter timing is another common method for realizing a linear VCPO. This method is illustrated in Figure 2. Starting with S_1 closed, S_2 open, and $V_3 - V_1 = V_s$ volts; voltage mode V_3 is at 2 IR volts and voltage mode V_1 is at $2IR - V_s$ volts. C_T is charged linearly to $V_1 - V_3 = V_s$ volts and then S_1 and S_2 change positions allowing C_T to be charged in the opposite direction to $V_3 - V_1 = V_s$ volts. This cycle produces a square wave of amplitude 2IR volts at voltage mode V_2. The frequency is derived below.

$$i = C_T \frac{d V_T}{dt}$$

$$\frac{T}{2} = \frac{C_T \Delta V_T}{I} = \frac{2C_T V_s}{I}$$

$$f = \frac{1}{T} = I/4C_T V_s \qquad (3)$$

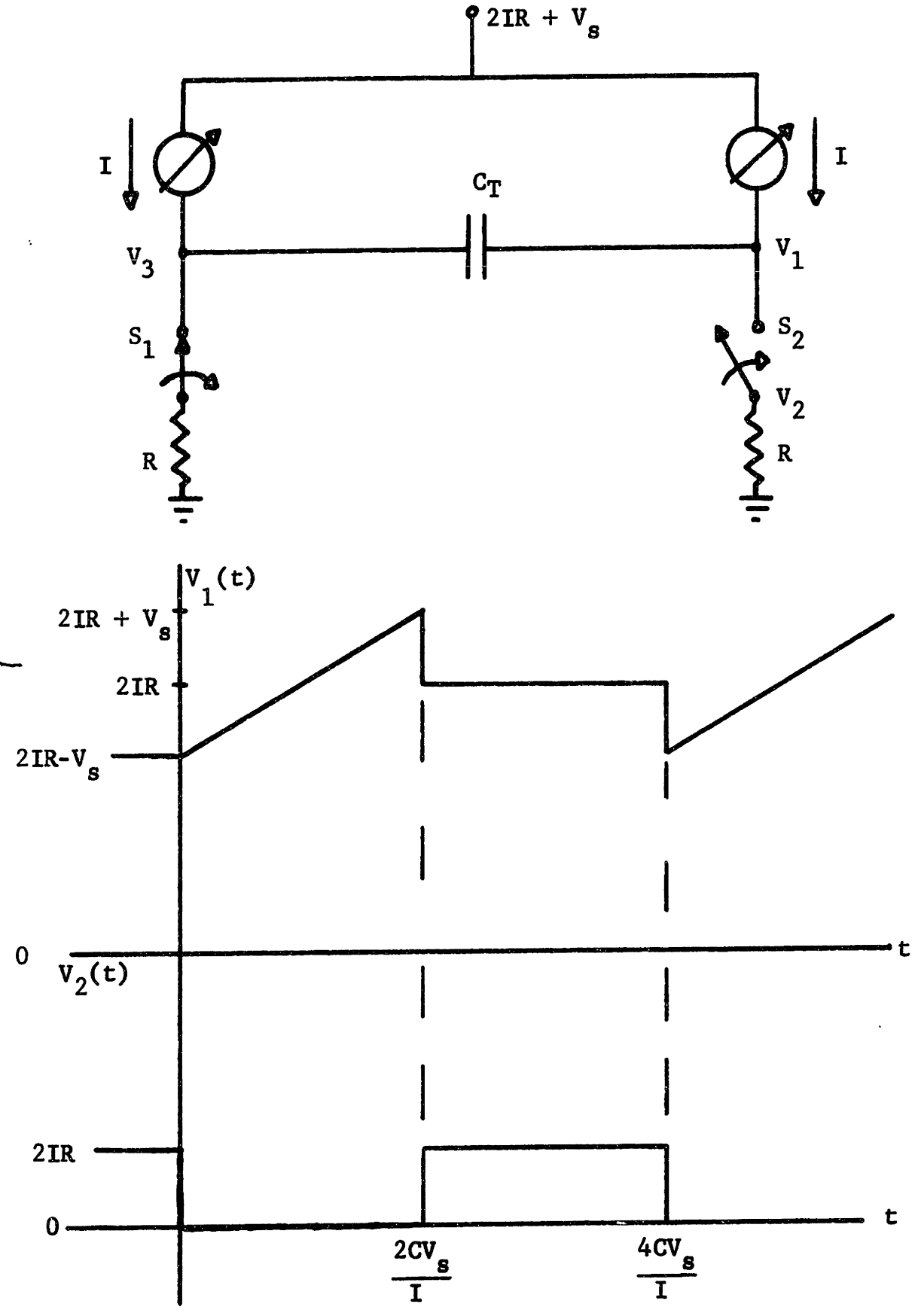

EMITTER TIMING

FIGURE 2

In a practical circuit S_1 and S_2 are replaced by regeneratively coupled transistors. At high frequencies the switching times of the transistors may be significant compared with the period of oscillation, causing some non-linearities in the charging and discharging of the timing capacitor. In this case the frequency will no longer be proportional to control voltage.

See Reference 3 for a circuit description of a VCPO using emitter timing.

1.23 A third way to build a linear VCPO is described in Reference 4 as an integrating voltage-to-frequency converter. A block diagram of this method is shown in Figure 3.

If the input to the integrator is a d-c voltage, its output is a negative going ramp whose slope is proportional to V_i. When V_L reaches E_R the level detector triggers the pulse generator and a pulse of fixed amplitude E and duration T is subtracted from V_c. This causes the output of the integrator to reverse direction and head toward its initial value. The frequency is derived below by referring to the wave forms shown in Figure 3.

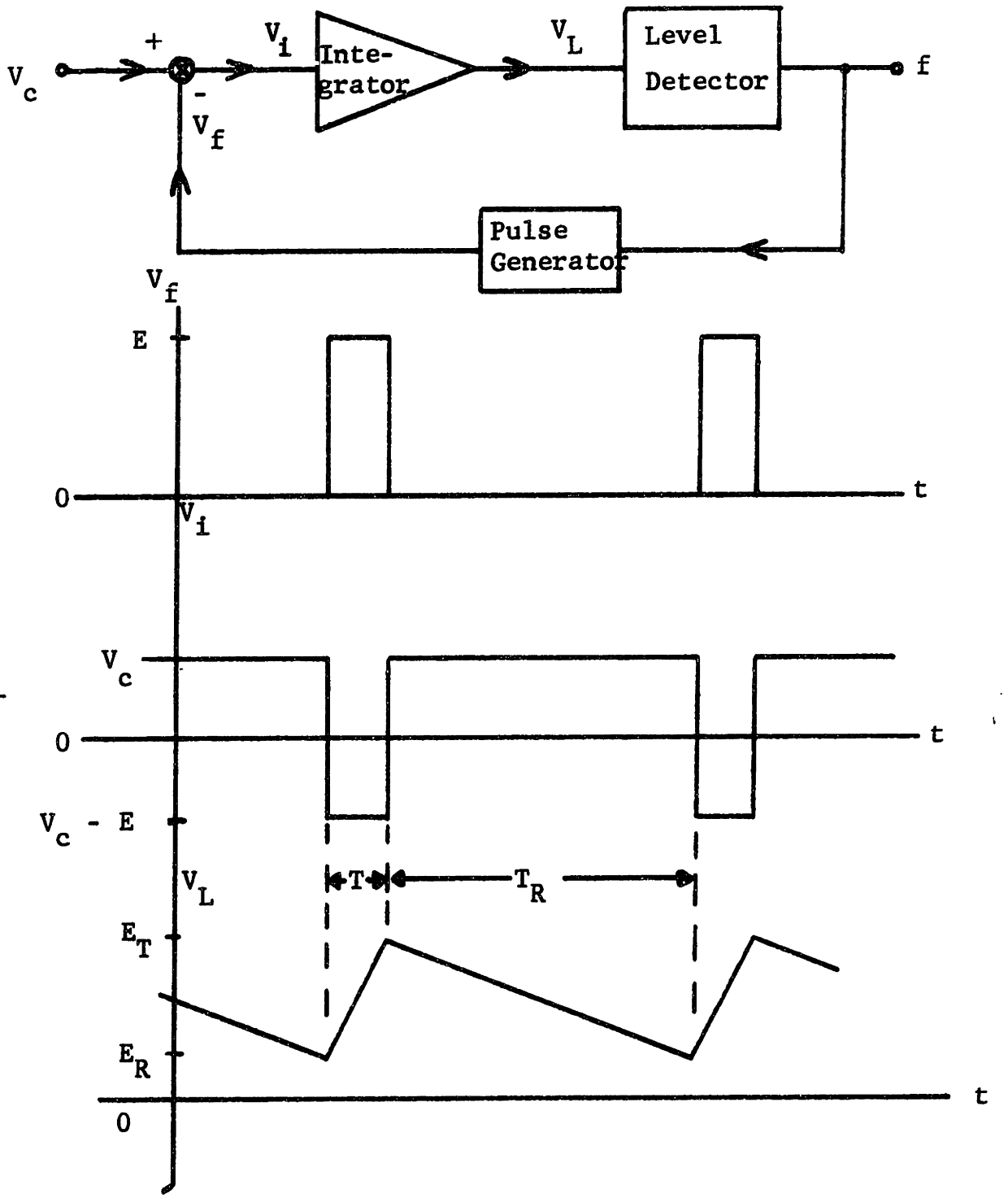

INTEGRATING VCPO

FIGURE 3

$$\text{Period} = P = T_R + T$$

$$V_L = m \int V_i dt \qquad \text{where m is the integration constant}$$

$$E_R - E_T = mV_c T_R$$

$$E_T - E_R = m(V_c - E)T$$

$$mV_c T_R = m(E - V_c)T$$

$$T_R = \frac{(E - V_c)T}{V_c}$$

$$P = T + \frac{T(E - V_c)}{V_c} = \frac{TE}{V_c}$$

$$f = 1/P = V_c/TE \qquad (4)$$

This method does not work well at high frequency because the rise time of V_f becomes comparable to T. In order to make the area of the pulse large enough to exactly reset the integrator, trouble is encountered with the pulses in V_f overlapping at the high end of the desired frequency range.

2.0 DISCUSSION OF SYSTEM DEVELOPED

The high frequency limitations of the circuits discussed in Section 1.2 are due to the fact that the components which determine the accuracy of the transfer function must operate at the output frequency. In order to achieve the design goals, a system was developed which would allow the accuracy to be governed by circuits which operate at a frequency two decades lower than the output frequency.

2.1 Analysis of Simplified System

To explain the operation of this system, the simplified block diagram of Figure 4 will be considered first. P represents a nonlinear VCPO whose transfer function varies with frequency. By looking at the transfer function for the block diagram of Figure 4, which is derived below, assuming the closed loop is stable, it can be seen that the effect of enclosing P by the feedback loop is to make the PRF of the closed loop system proportional to control voltage.

$$f = \frac{PAe_c}{1 + PAB} \tag{5}$$

$$\text{If} \quad |PAB| >> 1 \tag{6}$$

$$f \approx B^{-1} e_c \tag{7}$$

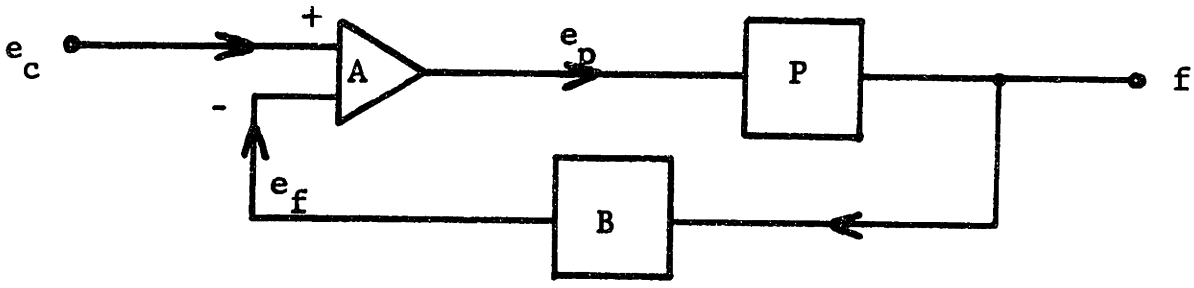

A => Difference Amplifier

P => VCPO

B => Frequency to Voltage Converter

SIMPLIFIED BLOCK DIAGRAM

FIGURE 4

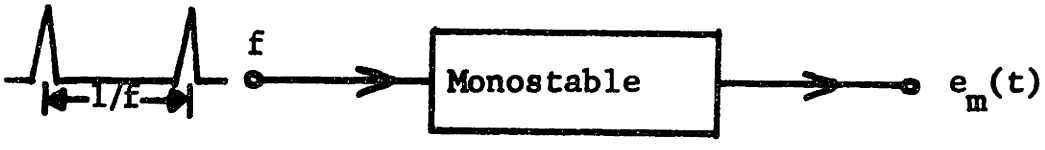

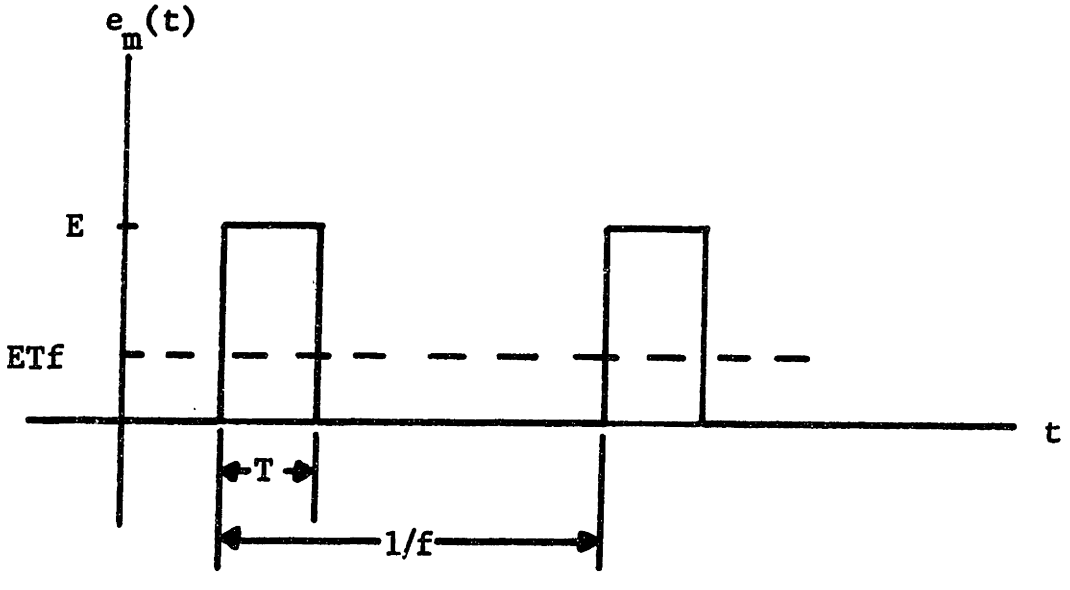

MONOSTABLE

FIGURE 4.5

The feedback voltage, e_f, regulates e_p in such a way as to compensate for the non-linearities of **P**. If the frequency goes below the desired value for a given e_c, the feedback voltage will drop and this will cause e_p to increase thus raising the frequency back towards the desired value; and vice versa.

It should be emphasized that B, the transfer function of the frequency to voltage converter, must be a constant in order for the frequency to be proportional to control voltage.

2.2 The Feedback Path

B can be realized in two parts. The first part is a monostable multivibrator whose output voltage waveform has a d-c value proportional to its driving frequency, as shown in Figure 4.5. The d-c value of $e_m(t)$ is ETf. The second part of B is a low pass filter which passes the d-c value of $e_{in}(t)$ and greatly attenuates the fundamental, f, and all harmonics.

With this arrangement for the frequency to voltage converter, B has the value ET; therefore, ET must be constant. If the monostable operates at the output frequency, it will be difficult to make ET a constant because the rise time of $e_m(t)$ becomes comparable to T. Variations in the rise time

from pulse to pulse will cause ET to vary significantly. The monostable is run saturated to hold E constant, and changes in the storage time from pulse to pulse at high frequency will cause significant variations in ET.

The situation can be remedied by dividing the output frequency by 100 before it is fed to the monostable. This will allow the monostable to run at a lower frequency where variations in the rise time and storage time will not cause significant variation in ET. If S is the scale of the frequency divider, B becomes ETS^{-1}; and this must be a constant for the system to have a proportional voltage to frequency transfer function.

2.3 Analysis of the Complete System

The complete system is shown in Figure 5, where the feedback path is separated into the three components discussed in Section 2.2. The closed loop transfer function is derived in Equations 8 - 12, with the assumption that the system is stable.

$$\frac{f}{e_c} = \frac{AP}{1 + APDMQ} \tag{8}$$

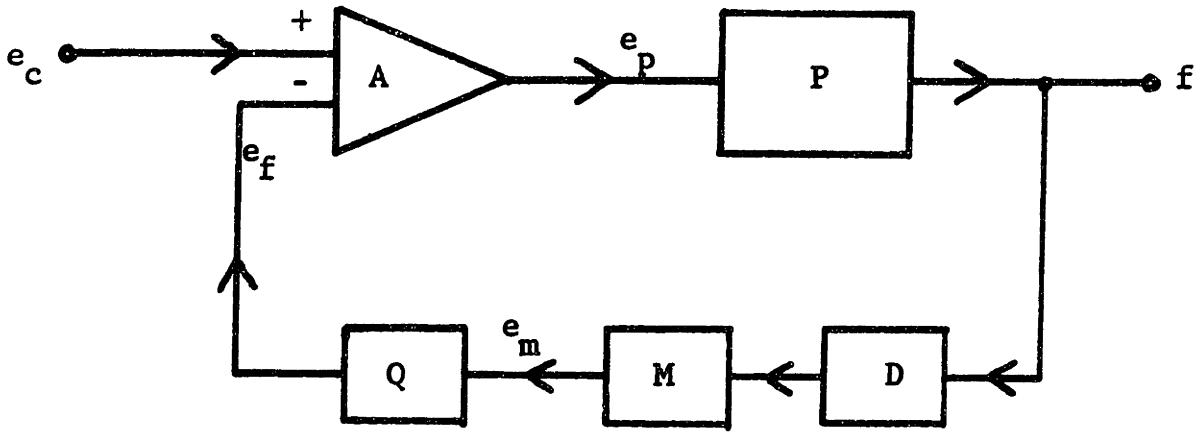

A => Difference Amplifier
P => Nonlinear VCPO
D => Frequency Divider
M => Monostable
Q => Low Pass Filter
e_c => Input Control Voltage
f => Output Frequency

COMPLETE SYSTEM

FIGURE 5

$$\text{If} \quad |APDMQ| \gg 1 \tag{9}$$

$$f \approx \frac{e_c}{DMQ} \tag{10}$$

Assuming the low pass filter is ideal

$$e_f/f = DMQ = ETS^{-1} \tag{11}$$

and by combining Equations 10 and 11

$$f \approx e_c/ETS^{-1} \tag{12}$$

Figure 5 and Equations 8 - 12 will be referred to in the following sections (2.31 - 2.37) which deal with various characteristics of the system's performance.

2.31 System Stability

The system of Figure 5 is stable if the poles of Equation 8 all lie in the left half plane. For the filter used in this system Q(s) is:

$$Q(s) = \frac{1}{(s\tau_1 + 1)(s\tau_2 + 1)} \tag{13}$$

where $\tau_1 = 6.4 \times 10^{-4}$sec., $\tau_2 = 2.7 \times 10^{-3}$sec. Let

$$APDM = H(s) \tag{14}$$

By substituting Equations 13 and 14 into Equation 8 it can be seen that the system is stable if the zeros of Equation 15 are in the left half plane.

$$1 + \frac{H(s)}{(\tau_1 s + 1)(\tau_2 s + 1)} = 0 \qquad (15)$$

It is very difficult to get an analytic expression for H(s), but the following approximations are good for the circuits used in realizing this system. The difference amplifier gain is down 3 db at 100 KHz, so let A(s) be:

$$A(s) = \frac{G}{(\tau_3 s + 1)} \qquad (16)$$

where $\tau_3 = 1.59 \times 10^{-7}$ sec.

and G = d-c gain = 100 for this system.

The combination PMD will have a very high frequency zero, but the effects of this zero will be neglected with respect to the pole of A. PMD will also have a small time delay, but this will also be neglected with respect to the pole of A. The magnitude of PDM in the frequency range of interest is 2. Considering PDM to be a constant value of 2, H(s) is 2A(s) and Equation 15 becomes:

$$1 + \frac{2G}{(\tau_1 s + 1)(\tau_2 s + 1)(\tau_3 s + 1)} = 0 \qquad (17)$$

Applying the Nyquist criterion to Equation 17, it is seen that the point -1/G must lie outside the shaded area of Figure 6 for the system to be stable. Since -1/G = -.01 the system is stable. In fact, 1/G must be greater than 9.6×10^{-5} for stability so the system is stable for any positive G less than 1.04×10^{4}.

2.32 Choosing the Transfer Function

Suppose that the desired closed loop transfer function is given in Equation 18 as:

$$f = Ke_c \tag{18}$$

K is a constant

The approximate transfer function for the closed loop system is given in Equation 10 as:

$$f \approx \frac{e_c}{DMQ} \tag{18.5}$$

Since the low pass filter greatly attenuates the fundamental (fS^{-1}) of $e_m(t)$ and passes the d-c value, ($ETfS^{-1}$), of $e_m(t)$ with a gain of 1, DMQ can be considered a constant equal to ETS^{-1}. The result of combining Equations 18 and 18.5 is:

$$K = (ET)^{-1}S \tag{19}$$

or

$$f = (ET)^{-1}Se_c \tag{20}$$

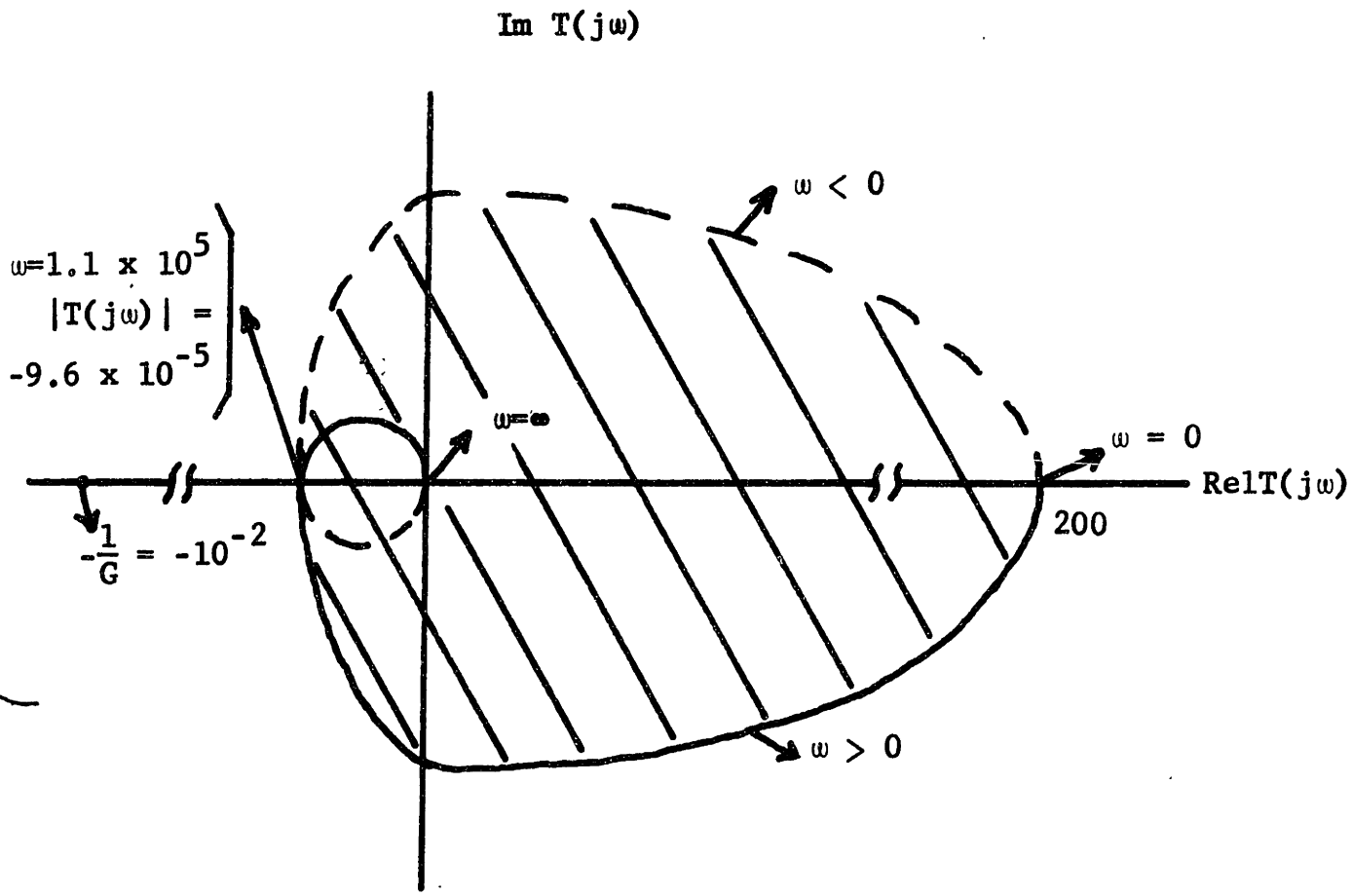

$$T(s) = 2/(\tau_1 s + 1)(\tau_2 s + 1)(\tau_3 s + 1)$$

NYQUIST PLOT

FIGURE 6

The output frequency is proportional to control voltage as can be seen from Equation 18, which is the desired transfer function. In this system K was chosen as 10^7 Hz/volt.

2.33 Accuracy of the Transfer Function

In discussing the accuracy of the transfer function of Figure 5, it will be necessary to decide what is meant by accuracy. The error in the output frequency is defined in Equation 21 as the percentage deviation of the actual frequency, f, from the desired value, Ke_c, for any particular control voltage.

$$\delta_f(e_c) \triangleq \left[\frac{f - Ke_c}{Ke_c}\right] 100 = \left[\frac{f(e_c)}{Ke_c} - 1\right] 100 \qquad (21)$$

where δ_f is the % error in f.

To evaluate δ_f Equation 8 must be solved for f in terms of e_c. Since it is not possible to do this but it is possible to solve Equation 8 for e_c as a function of f, the error of the closed loop system will be calculated as a percentage error in e_c. This percentage error is called $\delta_\ell(f)$ and is defined in Equation 22.

$$\delta_\ell(f) \triangleq 100 \left[\frac{e_c(f)}{fK^{-1}} - 1\right] \qquad (22)$$

It can be readily shown that $\delta_f(e_c) = -\delta_\ell(f)$ for any input output pair of the closed loop system. (See Appendix A-1).

Equation 8 is solved for e_c assuming that DMQ is a constant equal to ETS^{-1} and that the gain of the difference amplifier is G.

$$\frac{f}{e_c} = \frac{AP}{1 + APDMQ} \tag{8}$$

$$\frac{f}{P} + fADMQ = e_c A$$

$$d_c(f) = \frac{e_p(f)}{G} + fETS^{-1} \tag{23}$$

In order to evaluate the effectiveness of the feedback in improving on the accuracy of the nonlinear oscillator, P, it will be advantageous to express $\delta_\ell(f)$ in terms of the percentage error that would be obtained if just the nonlinear VCPO was used. If the nonlinear oscillator was used, the transfer function would be $f = e_p P$ where P represents a graph or table relating input output pairs of the nonlinear VCPO. Because P is nonlinear, it will have a different value for each input output pair.

Suppose the closed loop is calibrated at f_c to give zero error in the output frequency. The desired transfer function for P

would thus be given by Equation 24.

$$f = \frac{f_c}{e_p(f_c)} \; e_p(f) = K_p e_p(f) \tag{24}$$

where K_p is a constant.

The percentage error in P is defined as $\delta_p(f)$:

$$\delta_p(f) \triangleq 100 \left[\frac{e_p(f)}{f K_p^{-1}} - 1 \right] \tag{25}$$

ETS^{-1} is evaluated from Equation 23 in terms of f_c:

$$ETS^{-1} = \frac{e_c}{f_c} - \frac{e_p(f_c)}{f_c G}$$

$$= K^{-1} - \frac{K_p^{-1}}{G} \tag{26}$$

$\delta_\ell(f)$ can be calculated by substituting Equation 26 into Equation 23 and using the results in Equation 22.

$$\delta_\ell(f) = \frac{100K}{G} \left[\frac{e_p(f)}{f} - K_p^{-1} \right]$$

$$= \frac{K \delta_p(f)}{G K_p} \tag{27}$$

In this system G = 100 and $K/K_p = 1/2$ so the effect of the feedback is to divide percentage errors in P by 200. Therefore, P can deviate by as much as 200% from the desired

transfer function, and the closed loop system will still meet the design goals.

2.34 Effects of Parameter Changes on Accuracy

The accuracy of the closed loop system changes when the parameters of the component blocks change. It is useful to study the effect on accuracy of changes in the performance of some blocks in order to see which parameters must be tightly controlled when the system is realized.

2.341 Difference Amplifier Gain

Let the difference amplifier gain change from G to ϵG. From Equation 27 it can be readily seen that:

$$\delta_\ell(f) = \frac{K\delta_p(f)}{\epsilon G K_p} \qquad (28)$$

If ϵ is greater than one, the change in G will not be harmful to system performance as long as ϵG is less than 1.04×10^4 at which point the system will be unstable. If ϵ is less than one, the system loses accuracy. Since the largest magnitude of $\delta_p(f)$ is 30%, it is seen from Equation 28 that the minimum G can be is 15 to still have one percent accuracy.

2.342 Shifts in d-c Level of e_p

Suppose that the difference amplifier has some difference mode output due to common mode input. This will cause e_p to be $A(e_c - e_f) + c$ where c is the difference mode output due to common mode input. The errors due to c can be calculated with the aid of Figure 7.

$$e_p(f) = G(e_c - e_f) + c$$

$$= G(e_c - fETS^{-1}) + c \qquad (29)$$

$$e_c = \frac{e_p(f)}{G} + fETS^{-1} - \frac{c}{G} \qquad (30)$$

$$ETS^{-1} = \frac{e_c}{f_c} - \frac{e_p(f_c)}{Gf_c} + \frac{c}{f_cG}$$

$$= K^{-1} - \frac{K_p^{-1}}{G} + \frac{c}{f_cG} \qquad (31)$$

$$e_c = \frac{e_p(f)}{G} + fK^{-1} - \frac{fK_p^{-1}}{G} + \frac{c}{G}\left(\frac{f}{f_c} - 1\right) \qquad (32)$$

And from Equations 22 and 25

$$\delta_\ell(f) = \frac{K\delta_p(f)}{K_pG} + \frac{100Kc}{f_cG}\left[\frac{f - f_c}{f}\right] \qquad (33)$$

For this system c was negligible up to f_c and reached a peak of 100mV at f = 50 MHz. Since $\frac{100K}{f_cG} = .4$ for $f_c = 25$ MHz,

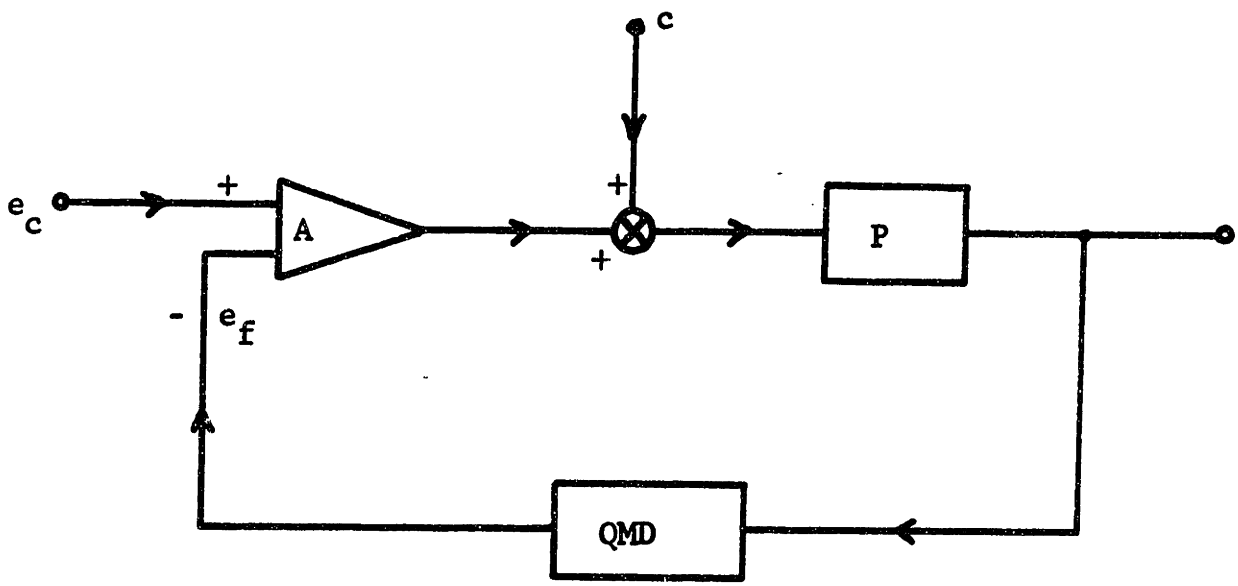

d-c OFFSET

FIGURE 7

the worst error due to c is .02%, which is of no concern compared to the design objective.

2.343 Changes in ETS^{-1}

Let ETS^{-1} change from ETS^{-1} to ϵETS^{-1}. Define the percentage change in ETS^{-1} as:

$$\delta_b \triangleq 100(\epsilon - 1)$$

Equation 23 now becomes

$$e_c(f) = \frac{e_p(f)}{G} + \epsilon f ETS^{-1} \tag{34}$$

and by using Equations 26, 22, and 25 in Equation 34, $\delta_\ell(f)$ becomes:

$$\delta_\ell(f) = \frac{K\delta_p(f)}{GK_p} + \delta_b\left[1 - \frac{K}{GK_p}\right] \tag{35}$$

Since $K/GK_p = .005$ for this system it can be seen that errors in ETS^{-1} add directly to the total closed loop error. Equation 35 is simply a mathematical verification of the statement made at the end of Section 2.2 that ETS^{-1} must be a constant for the closed loop system to have the proper transfer function.

2.35 F-M Modulation

If e_c is a low frequency sine wave, the output PRF will be F-M modulated. The desired output is:

$$f = K(L + N\sin\omega_m t) \tag{36}$$

if

$$e_c = L + N\sin\omega t \tag{37}$$

In order to see how well the modulating wave form is reproduced at the output, consider the response of the system to:

$$e_c = N\sin\omega_m t \tag{38}$$

where the center frequency, KL, has been subtracted out for simplicity. From Equations 8, 13, 16, and the fact that $DM = K^{-1}$ the closed loop transfer function can be written in the following way:

$$f(s) = \frac{(\tau_1 s + 1)\ (\tau_2 s + 1)\ GPe_c(s)}{(\tau_1 s + 1)(\tau_2 s + 1)(\tau_3 s + 1) + GPK^{-1}} \tag{39}$$

Since $s^n f(s)$ transforms to $\frac{d^n}{dt^n} f(t)$ for zero initial conditions (see Reference 5), Equation 39 can be converted to a third order linear differential equation with constant coefficients. The particular solution for f(t) to Equation 38 can be found by assuming the solution:

$$f(t) = C_1\cos\omega_m t + C_2\sin\omega_m t \tag{40}$$

and using the method of undetermined coefficients to solve for C_1 and C_2. The result of this operation is:

$$f \approx KN(1 - R^2C^2\omega_m^2)\sin\omega_m t$$

$$+ 3KNRC\omega_m\cos\omega_m t$$

$$\text{where} \quad RC = 1.68 \times 10^{-3} \text{ sec.} \qquad (41)$$

Equation 40 is an approximation in which $RC\omega_m$, $(RC\omega_m^2)$, $\tau_3(RC)^2\omega_m^3$ and $9(RC\omega_m)^2$ have been neglected in relation to 200 in the expressions for C_1 and C_2. This approximation is good to 5% or better for $f_m \leq 95$ Hz. At $f_m = 95$ Hz, Equation 41 is:

$$f(t) = 3KN\cos\omega_m t \qquad (42)$$

which shows that the system does not work well as a modulator.

If a filter, Q(s), is added to the input of the closed loop system, as shown in Figure 8, the modulation performance is greatly improved. It can readily be seen that this filter has no effect on the stability or accuracy calculations done in the previous sections.

Using Equation 39 with $e_c(s)$ replaced by $Q(s)e_c(s)$, the transfer function of Figure 8 is:

$$f(s) = \frac{GPe_c(s)}{(\tau_1 s + 1)(\tau_2 s + 1)(\tau_3 s + 1) + GPK^{-1}} \qquad (43)$$

Employing the same kind of procedure as followed in solving Equation 39, the time domain solution for f from Equation 43

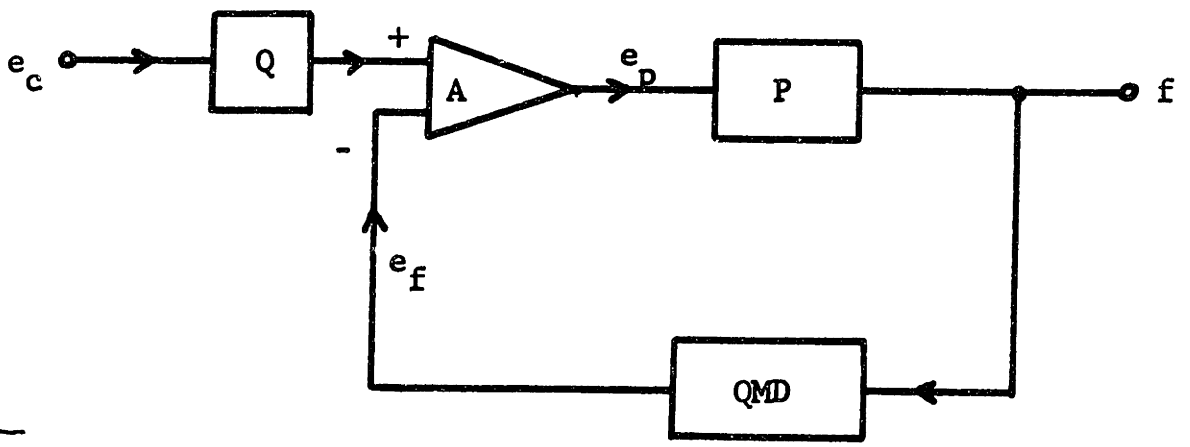

SYSTEM WITH INPUT FILTER

FIGURE 8

to the input of Equation 38 is:

$$f(t) = KN\sin\omega_m t - \frac{3KNRC\omega_m}{200} \cos\omega_m t \qquad (44)$$

The approximations used in arriving at Equation 44 are on the amplitudes of the sine and cosine terms and are good to 1% for $f_m \leq 95$ Hz.

At $f_m = 95$ Hz Equation 44 is:

$$f(t) = KN\sin\omega_m t - 0.015\ KN\cos\omega_m t \qquad (45)$$

which by comparison with Equation 42 is a substantial improvement in performance due to the addition of the input filter.

2.36 The Step Response of the System

The step response is another useful performance measure of the system. The response of e_p to a step change of control voltage will be calculated.

Equation 46 is derived from Equation 8 by setting $f(s) = Pe_p(s)$.

$$e_p(s) = \frac{A(s)\ e_c(s)}{1 + A(s)PDMQ(s)} \qquad (46)$$

Using Equations 13, 16, and the fact that PDM $\approx$ 2 for this system:

$$e_p(s) = \frac{(\tau_1 s + 1)(\tau_2 s + 1)\ G\ e_c(s)}{(\tau_1 s + 1)(\tau_2 s + 1)(\tau_3 s + 1) + 2G} \qquad (47)$$

$$\text{let}\quad e_c(t) = Cu_{-1}(t) \qquad (48)$$

Since τ_3 corresponds to a cut off frequency of 100 KH_z, the effects of this pole on the response of $e_p(t)$ will not be noticeable at times greater than 0.1ms after the step in control voltage occurs. The settling time will be determined primarily by τ_1 and τ_2 so that τ_3 can be taken as zero in Equation 47. This will also greatly simplify the calculation of $e_p(t)$. The approximate Equation for $e_p(s)$ becomes:

$$e_p(s) = \frac{(\tau_1 s + 1)(\tau_2 s + 1)\ G\ e_c(s)}{(\tau_1 s + 1)(\tau_2 s + 1) + 2G} \qquad (49)$$

Assuming zero initial conditions, the time domain solution for e_p can be constructed by Laplace Transform techniques. The answer is:

$$e_p(t) = \frac{C(2G - 1)}{2} e^{-\sigma_o t}\left[\frac{\sigma_o}{\omega_o}\sin\omega_o t + \cos\omega_o t\right]u_{-1}(t)$$

$$+ \frac{C}{2}\ u_{-1}(t) \qquad (50)$$

$$\text{where } \sigma_o = 890 \text{ sec}^{-1}$$

$$f_o = \frac{\omega_o}{2\pi} = 1.24 \text{ KHz}$$

Replacing the sine and cosine terms in Equation 50 by 1 gives a settling time of 11.1ms for $e_p(t)$ to be within 1% of its final value. Equation 50 also shows that there is an initial overshoot of $\frac{C(2G-1)}{2}$ in $e_p(t)$. G is about 100 for this

system so this is an initial overshoot of almost 200 times the final value.

When the input filter discussed in the previous section is added to the circuit, the transient response has more desirable characteristics. With the input filter in place, $e_p(s)$ is found from Equation 47 by replacing $e_c(s)$ by $e_c(s)/(\tau_1 s + 1)(\tau_2 s + 1)$:

$$e_p(s) = \frac{G\, e_c(s)}{(\tau_1 s + 1)(\tau_2 s + 1)(\tau_3 s + 1) + 2G} \qquad (51)$$

Employing the same approximations and methods as used in solving Equation 47, the solution for $e_p(t)$ from Equation 51 is:

$$e_p(t) = \frac{C}{2} u_{-1}(t) - \frac{C}{2} e^{-\sigma_o t} \left[\frac{\sigma_o}{\omega_o} \sin\omega_o t + \cos\omega_o t\right] u_{-1}(t) \qquad (52)$$

The settling time for $e_p(t)$ to reach 1% of its final value in Equation 52 is 5.15ms, and the peak overshoot is about equal to the final value. By comparison with the results for Equation 50 one can see that both the settling time and the overshoot are improved by using the input filter.

2.37 Ripple in the Feedback Voltage

There is a certain amount of ripple voltage in e_f due to the first harmonic of e_m which is passed by the filter.

This ripple voltage is amplified by the difference amplifier and appears at e_p causing the output frequency to be slightly modulated.

The amplitude of the ripple voltage can be estimated by multiplying the fourrier series coefficient for the fundamental of e_m by the gain of the low pass filter at this frequency. The results of these calculations are shown in Equation 53:

$$E_J(f_o) = \frac{2ET}{\tau_1 \tau_2 \, 4\pi^2 \, S^{-1} f_o} \tag{53}$$

where E_J = amplitude of ripple voltage

and f_o = output frequency.

The ripple voltage appearing at e_p is

$$E_{JP} = G \, E_J \tag{54}$$

The peak error in PRF due to modulation by E_{JP} is:

$$\delta_J(f_o) \triangleq 100\left(\frac{PGE_J}{f_o}\right) \tag{55}$$

Taking $P(5MH_z)$ to be a constant, 1.32×10^7, $\delta_J(f_o)$ is calculated for $f_o = 5\ MH_z$:

$$\delta_J(5MH_z) = 0.157\% \tag{56}$$

Equation 56 represents the worst jitter in the frequency range of interest because $\delta_J(f_o)$ is an inverse function of frequency.

3.0 DESCRIPTION OF CIRCUITS USED

3.10 The Oscillator

The free running oscillator, referred to as P in Figure 5, operates on the principle of ramp timing. In order to assure good performance at high frequencies, the level detection and set, reset pulse generation functions are accomplished in a manner to minimize the switching time of these functions.

The operation of the oscillator is explained with the aid of the simplified schematic shown in Figure 9. The charging current for the timing capacitor, C_T, is supplied by a voltage-controlled current source, Q-1. Q-2 and Q-3 form an a-c coupled Schmitt trigger which acts as level detector and set, reset pulse generator, Q-4 and Q-5 are a voltage comparator which supplies the discharge current for C_T and the output pulse.

Q-1 continuously charges C_T. During the charging interval Q-3 and Q-5 are on and Q-2 and Q-4 are off so that the capacitor voltage rises above ground. When this timing voltage reaches the positive threshold of the Schmitt trigger, Q-2 and Q-4 turn on, forcing Q-3 and Q-5 off. Q-4's collector

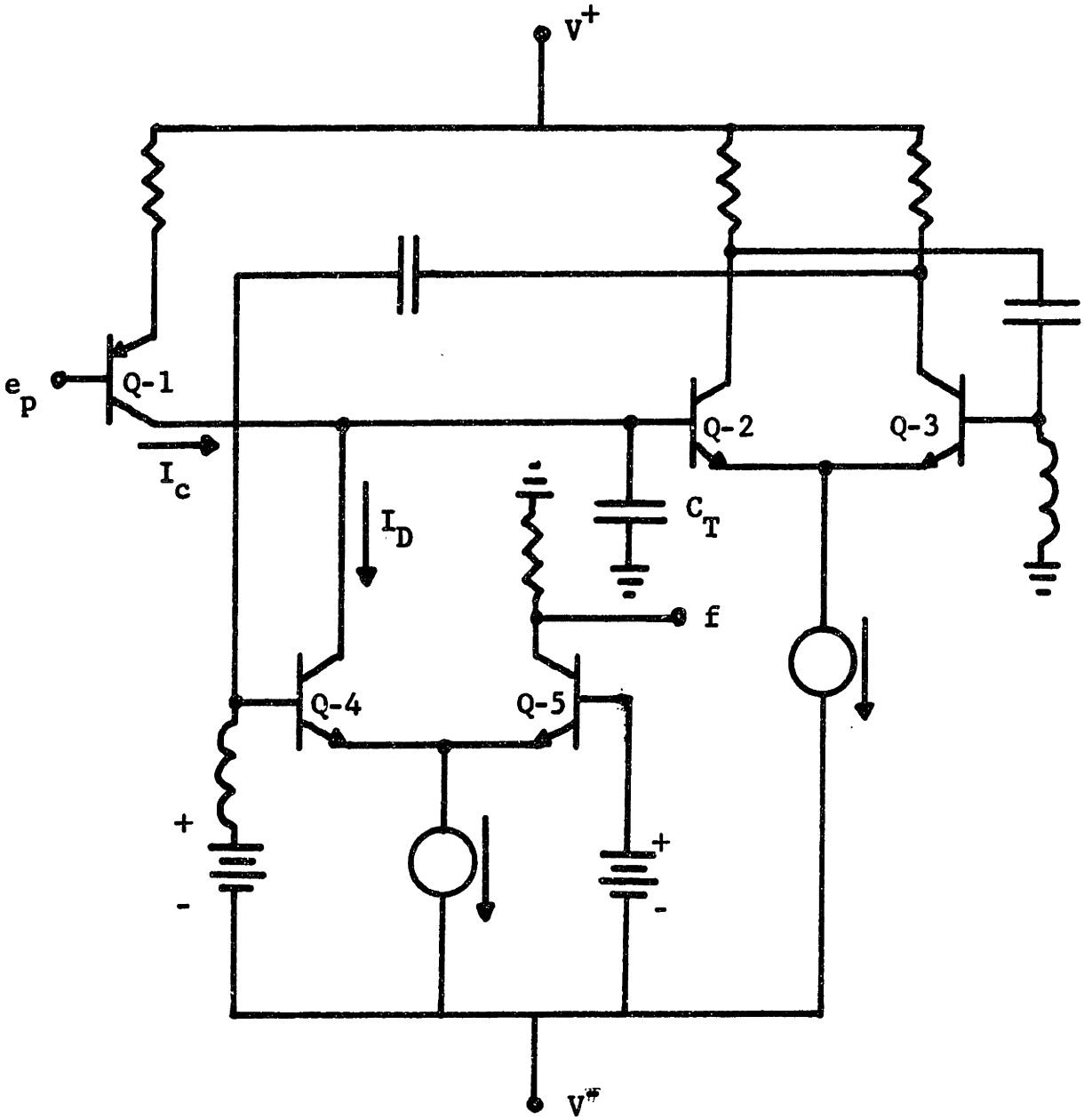

OSCILLATOR, P

FIGURE 9

current, which is always greater than I_c, discharges C_T toward the negative threshold of the Schmitt Trigger. When the negative threshold is reached, Q-3 and Q-5 turn on, while Q-2 and Q-4 turn off, allowing C_T to be recharged toward the positive threshold.

The frequency is varied by changing e_p. As e_p is moved toward ground, I_c increases and the frequency decreases.

This circuit works well at high frequency because a fast Schmitt Trigger is used as a level detector, and only the discharge current is switched on and off.

3.11 Some unsuccessful methods for realizing the oscillator were tried before the circuit of Figure 9 was designed. Two of these methods took the form of the Schmitt Oscillator shown in Figure 10. To see how this circuit works, assume that Q-1 is on and Q-2 is off. When the circuit is in this state, the zener translation of Q-1's collector voltage holds V_z below ground so that the timing capacitor is discharged through R_T. The circuit changes state when the voltage across C_T reaches the negative threshold of the Schmitt Trigger formed by Q-1 and Q-2 so that now V_z is above ground and C_T is charged back toward the positive threshold voltage

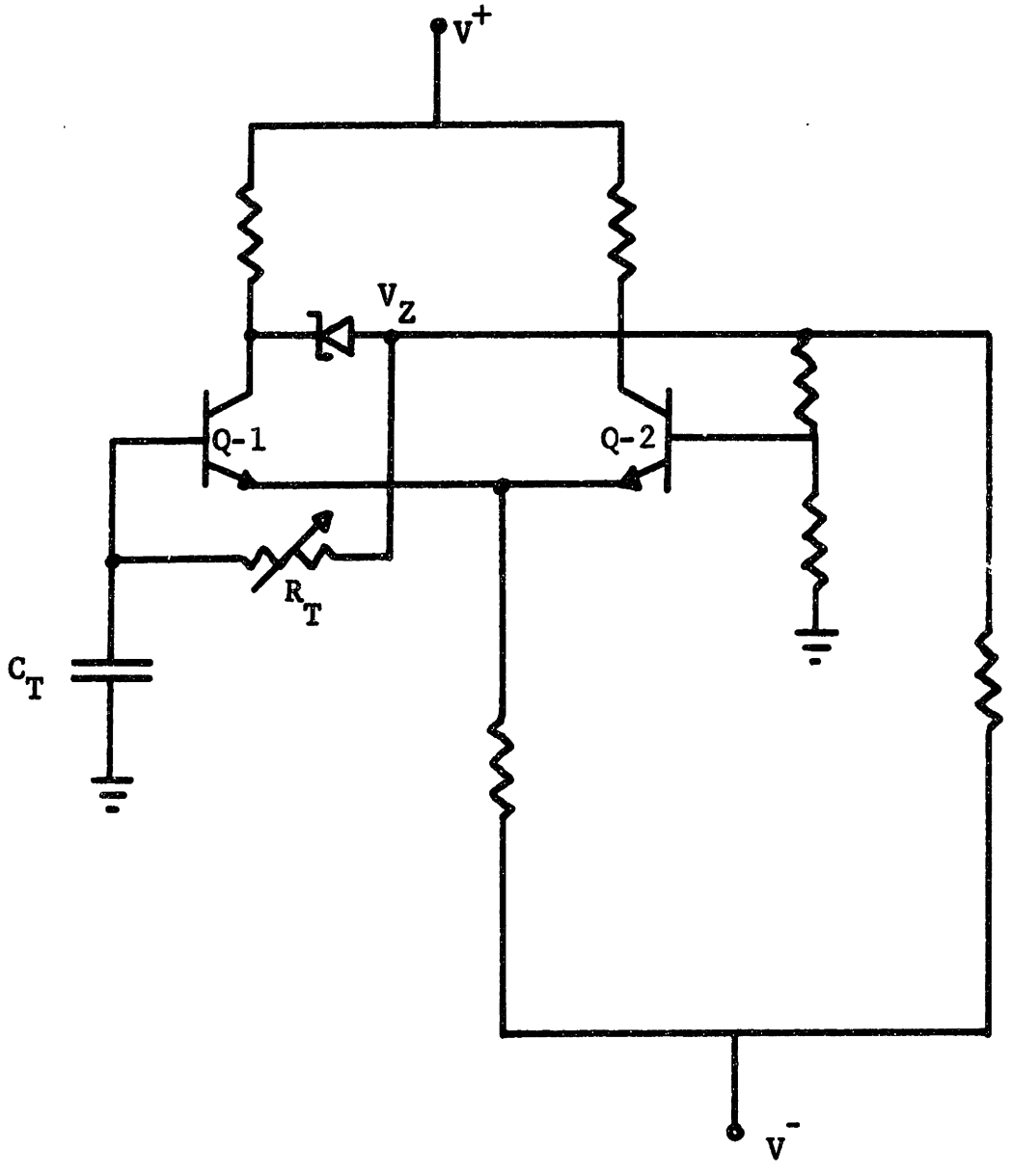

SCHMITT OSCILLATOR

FIGURE 10

where the circuit returns to its original state.

The frequency is varied by changing the $R_T C_T$ time constant. Since a voltage-controlled oscillator is desired, R_T could be a voltage variable resistor. The combination of a cadmium-sulfide photoresistor and an incandescent light bulb was tried. It was possible to get a decade variation of frequency in the range of interest with this combination; but when this oscillator was put in the closed loop of Figure 5, the system was unstable because the photoresistor-light bulb combination has a very long time constant that corresponds to a low frequency pole.

The dynamic resistance between the source and drain of a field effect transistor was also tried as a voltage controlled resistor by using the gate voltage as a control voltage. This method did not work at all. The problem seemed to be that current has to flow in both directions between the source and the drain so that these terminal voltages are both changing with respect to the gate voltage, causing great changes in the dynamic resistance when the current changes direction.

A method proposed by Rosenthal (see reference 6 for a description of this method) for a voltage-controlled pulse

modulator was also considered. After a careful study of the circuitry involved in realizing this type of oscillator, it was decided that it would not perform at high enough frequencies and no test circuits were designed.

3.2 The Monostable

The conventional monostable multivibrator shown in Figure 11 does not work well at high duty ratios or high frequencies because C_T does not have time to fully recharge from one cycle to the next. The operation of the circuit in Figure 11 is a follows. Q-1 turns off and Q-2 turns on when a negative trigger pulse is applied at the base of Q-1. This causes C_T to be discharged through Q-2 and holds Q-1 off. When the current in C_T reaches a low level, Q-1 turns back on and C_T is recharged by Q-1's base current. Since this base current is small compared to Q-2's collector current, it will take a longer time to recharge C_T to V^+ than it did to discharge it through Q-2. This will cause trouble when the duty ratio is high.

The circuit shown in Figure 12 was recommended to me by James K. Skilling Development Engineer at the General Radio Company, to overcome the problems of a conventional mono-

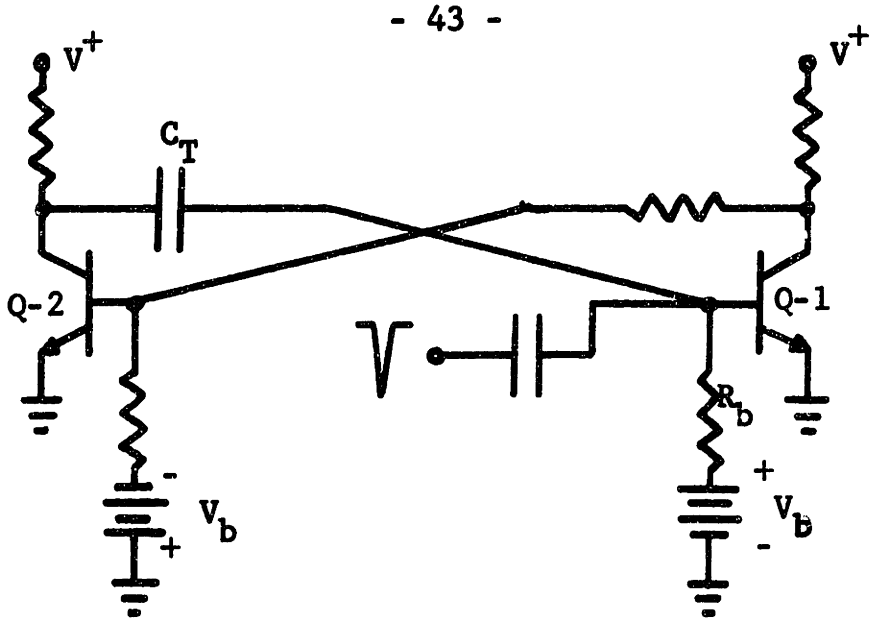

CONVENTIONAL MONOSTABLE

FIGURE 11

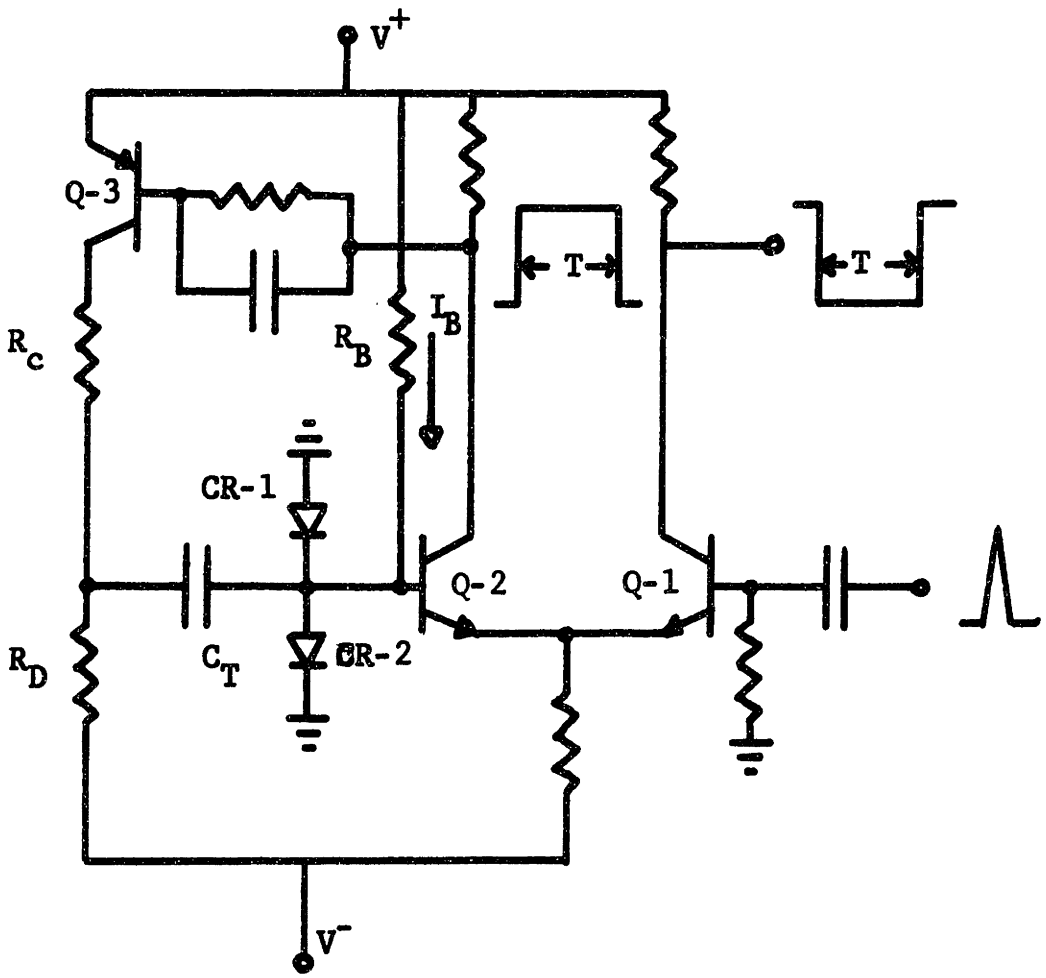

MONOSTABLE

FIGURE 12

stable in the frequency range and duty ratio required in this system. In order to see the advantages of the monostable used in this system, the circuit of Figure 12 will be explained. Normally Q-1 is off and Q-2 and Q-3 are on. When a positive trigger pulse is applied at the base of Q-1, Q-2's emitter is raised above the anode potential of CR-2 causing Q-2 and Q-3 to turn off while Q-1 is turned on. Because Q-3 is off, C_T discharges through R_D, which forward biases CR-1 setting up a constant current, I_B, in R_B. When the current in C_T drops below I_B, CR-2 is forward biased, which turns Q-2 back on and Q-1 off. Q-3 is now turned on to saturation with initial overdrive which rapidly recharges C_T through R_C so that the circuit is ready for the next trigger pulse.

This circuit produces a constant, stable time interval, T, because C_T is rapidly recharged and because the current I_B that determines the end of the time interval is held uniform by V^+ and CR-1.

To complete the design of the monostable, the output stage shown in Figure 13 is used to set the amplitude, E, of $e_m(t)$. During the time interval, T, Q-1 is on and saturated. The amplitude E is controlled by zener diode CR-3 which has

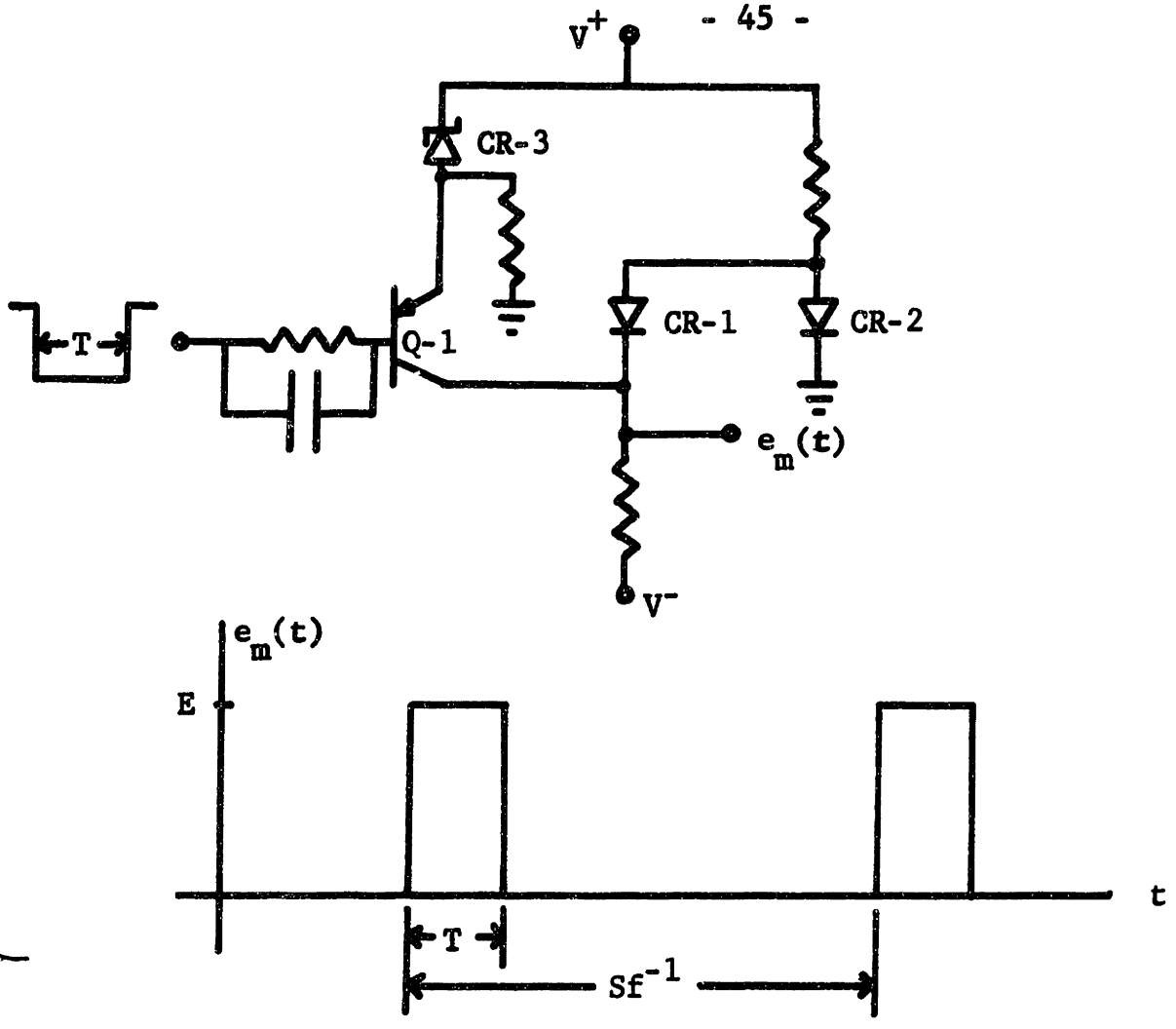

OUTPUT STAGE OF MONOSTABLE

FIGURE 13

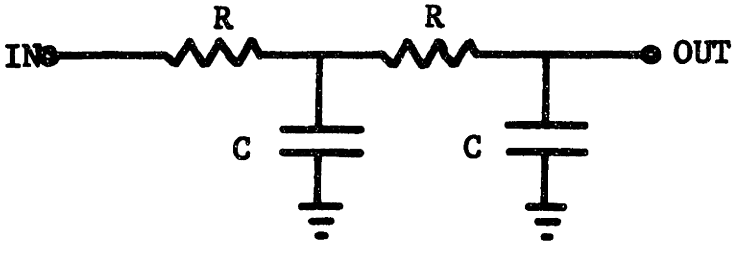

FILTERS

FIGURE 14

a 0.01% per °C temperature coefficient to prevent changes in the zener voltage with different duty ratios of $e_m(t)$. When Q-1 is off the ground level of $e_m(t)$ is set by CR-1 and CR-2 which have equal currents flowing in them.

3.3 The Difference Amplifier

The difference amplifier, A, used in this system is a conventional long tail pair. The differential gain at low frequencies is 100 and the amplifier has a 3db cut off frequency of 100 KHz.

3.4 Filters

The input filter and the feedback filter are two stage RC filters of the type shown in Figure 14. Both filters have poles at 59 Hz and 248 Hz. The input filter is scaled down in impedance by a factor of 100 with respect to the feedback filter to reduce loading on the control voltage.

3.5 The Frequency Divider

Two General Radio Company 1396-A Decade Prescalors are used for the frequency divider, D. This combination provides at division of frequency by 100 which is referred to as S in Chapter 2.

3.6 Complete Schematic

A complete schematic of the circuits used in this system, excluding the frequency divider, is included in the appendix on page 66, in Figure 27.

4.0 EXPERIMENTAL RESULTS

In this chapter several of the calculations in Chapter 2 are compared with measurements of the actual circuit performance.

4.1 D-C Linearity

The accuracy of the closed loop transfer function can be predicted as a function of the nonlinearity of the oscillator, P, by using Equations 25 and 27. Equation 27 is plotted as the upper curve in Figure 15 by using measured data from the oscillator, P, to evaluate $\delta_p(f)$.

The accuracy of the closed loop system can also be expressed as:

$$\delta_\ell(f) = 100 \left[\frac{e_c(f)\ K}{f} - 1 \right] \qquad (57)$$

Equation 57 is plotted as the lower curve in Figure 15 from measured values of $e_c(f)$ and f taken from the closed loop system.

Equation 27 does not appear to be an accurate prediction of the error in the closed loop transfer function, as can be seen from Figure 15. The measured value of e_c for the closed

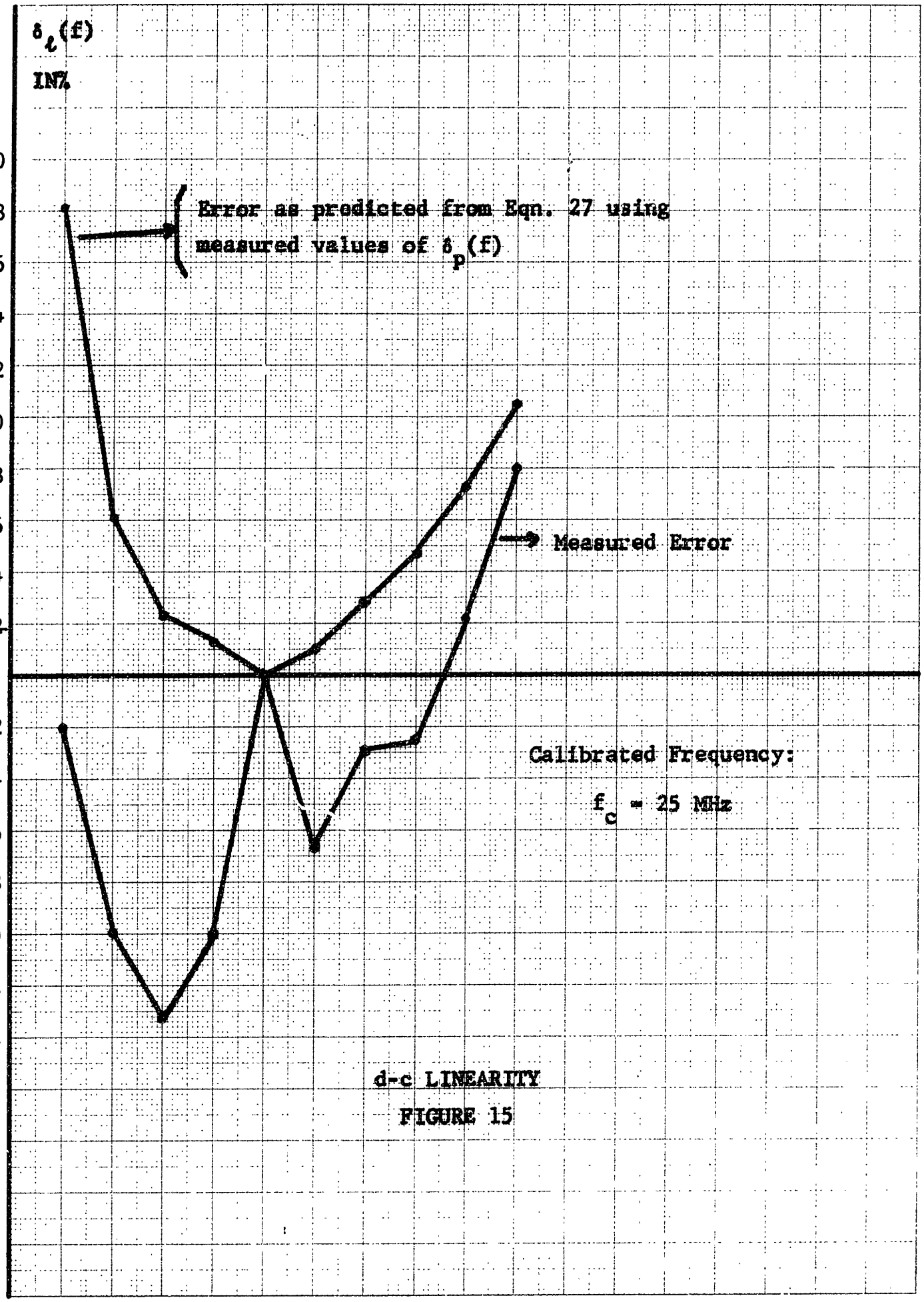

d-c LINEARITY

FIGURE 15

loop system is less than the value predicted by Equation 27 at all frequencies except the calibration frequency. This indicates that e_p has a small positive value when e_c is zero. This fact was verified by setting e_c to zero volts and observing that the oscillator, P, was still operating at some low frequency.

For frequencies lower than the calibration frequency Equation 33 would be preferable to predict the error, where the value of e_p for $e_c = 0$ would be c in equation 33. The second term in Equation 33 is negative for $f < f_c$ and this will lower the predicted error and bring it closer to the value observed in the closed loop system. In the actual circuit e_p has been translated positive to be compatible with the output level of the difference amplifier. Therefore, it is difficult to get an accurate measure of c due to this translation, and Equation 33 was not plotted.

For $f > f_c$ the second term in Equation 33 is positive and will tend to make the predicted error even higher than the value given by Equation 27. However, there is another effect which overides the effect of c at frequencies greater than f_c. This is the fact that E, the amplitude of the

monostable output, decreases at high frequencies due to the temperature coefficient of the zener diode in the output stage of the monostable. This change in E is accounted for in Equation 35. The second term in Equation 35 is negative for a decrease in E relative to its value at the calibration frequency. This will lower the predicted error and reduce it toward the measured value.

The best error prediction would be a combination of Equations 33 and 35 as shown in Equation 58.

$$\delta_\ell(f) = \frac{K\delta_p(f)}{K_p G} + \frac{100Kc}{f_c G}\left[\frac{f - f_c}{f}\right] + \delta_b \qquad (58)$$

Since it is difficult to obtain meaningful numbers for c and δ_b, this equation was not plotted.

It should be pointed out that the measured error was well within the design goals of $\pm$ 1%.

4.2 F-M Modulation Characteristics

To test the modulation capabilities of the closed loop system, $e_c(t)$ was set to $2.5 + \sin 2\pi f_m t$ volts. The output waveform was fed into a demodulator with a constant of proportionality equal to K^{-1} so that the amplitude of the

demodulated waveform had a scale factor of one with respect to the modulating voltage in $e_c(t)$. This allows a direct comparison between the modulating voltage and the demodulated output frequency on an oscilloscope, which is done in Figures 16 - 19.

In Figure 16 the upper trace is the a-c component of control voltage and the lower trace is the demodulated output frequency for f_m = 10 Hz; without the input filter added to the closed loop system. Equation 41 may be used to predict the output of the demodulator and yields the ratio of amplitudes of the lower trace to the upper trace as 1.04 and the phase lead of the lower trace to be 17.9 degrees with respect to the upper trace. The data from Figure 16 shows the amplitude ratio to be about 1.05 and the phase lead as 19.4 degrees.

In Figure 17 the upper trace is the modulating voltage for f_m = 100 Hz and the lower trace is the demodulated output frequency without the input filter. Equation 41 predicts an amplitude ratio of 3 and a phase lead of 90° for f_m = 95 Hz. Figure 17 shows that these results actually occur at 100 Hz in the closed loop system.

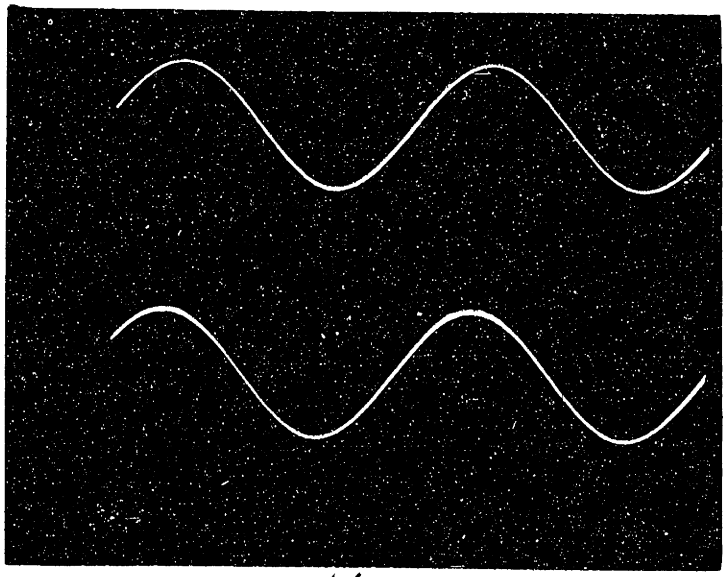

16

UPPER TRACE--MODULATING VOLTAGE AT 0.5 VOLTS/CM

LOWER TRACE--DEMODULATED OUTPUT AT 0.5 VOLTS/CM
TIME SCALE--20 ms/cm

10 Hz MODULATION WITHOUT INPUT FILTER

FIGURE 16

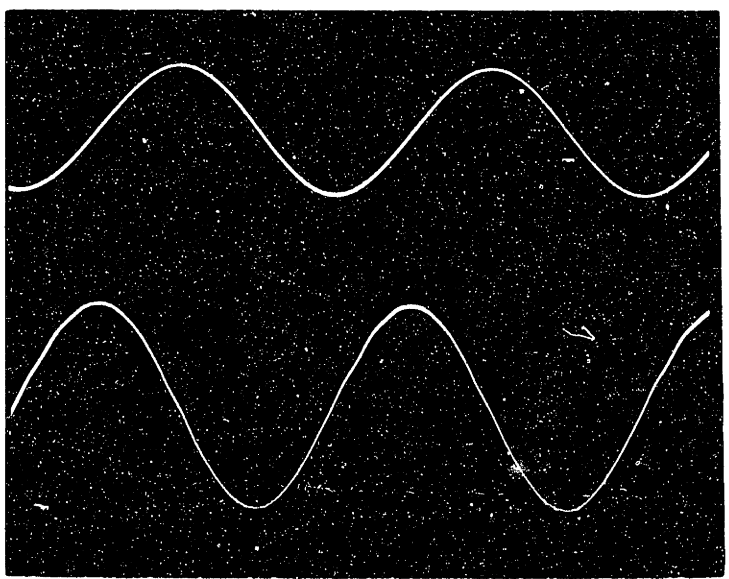

17

UPPER TRACE--MODULATING VOLTAGE AT 0.5 VOLTS/CM

LOWER TRACE--DEMODULATED OUTPUT AT 1.0 VOLTS/CM
TIME SCALE--2 ms/cm

100 Hz MODULATION WITHOUT INPUT FILTER
FIGURE 17

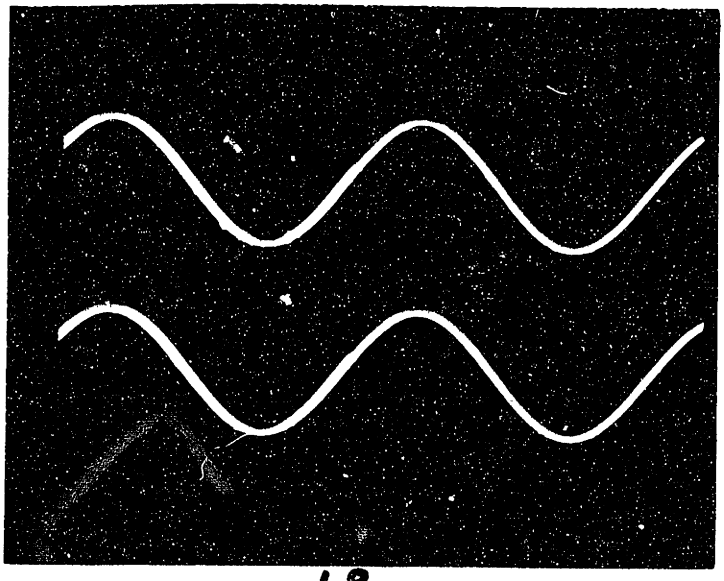

18

UPPER TRACE--MODULATING VOLTAGE AT 0.5 VOLTS/CM

LOWER TRACE--DEMODULATED OUTPUT AT 0.5 VOLTS/CM
TIME SCALE--20ms/cm

10 Hz MODULATION WITH INPUT FILTER ADDED

FIGURE 18

100 Hz MODULATION WITH INPUT FILTER ADDED

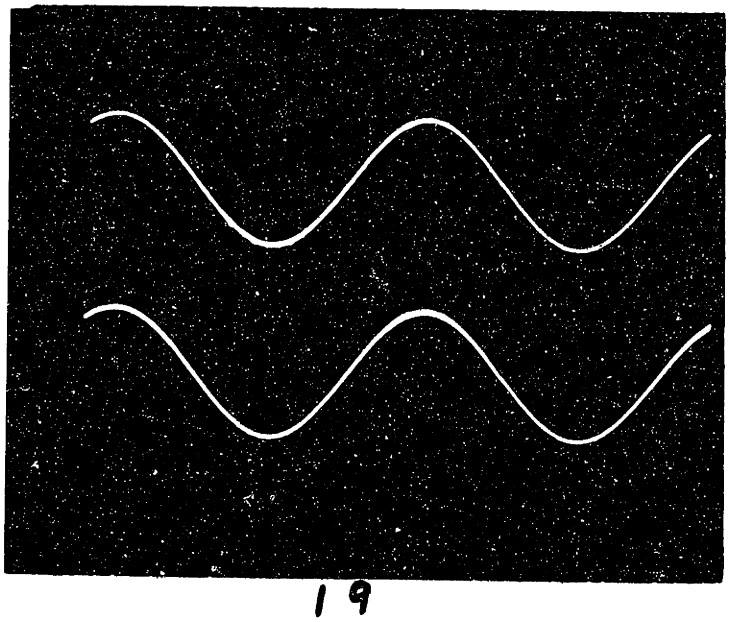

19

UPPER TRACE--MODULATING VOLTAGE AT 0.5 VOLTS/CM

LOWER TRACE--DEMODULATED OUTPUT AT 0.5 VOLTS/CM
TIME SCALE--2 ms/cm
FIGURE 19

When the closed loop system has the input filter added, Equation 44 can be used to predict the performance. This equation indicates that for f_m up to 100 H_z the demodulated output frequency should have very nearly the same amplitude and phase as the modulating voltage. Figure 18 shows the two waveforms for f_m = 10 Hz, and Figure 19 shows them for f_m = 100Hz. As can be seen from these Figures, the two waveforms are so nearly identical that no measurement of their difference can be made by visual comparison.

The data presented in this section shows that the measurements of the closed loop system are in close agreement with the theory presented in Chapter 2 for the F-M modulation characteristics. In particular, the addition of the input filter improves the modulation characteristics of the system.

4.3 Step Response

Figures 20 and 21 show the step response of $e_p(t)$ without the input filter. The upper trace is the step change in control voltage and the lower trace is the response of $e_p(t)$ to this change in control voltage. Equation 50 gives the calculated response of $e_p(t)$ to a step change of

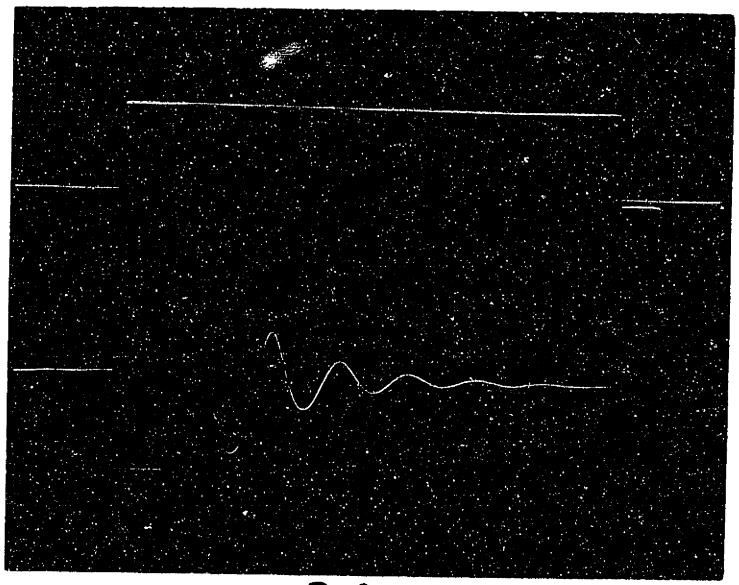

20

UPPER TRACE--STEP CHANGE IN e_c AT 0.2 VOLTS/CM
LOWER TRACE--RESPONSE OF e_p AT 2 VOLTS/CM
TIME SCALE--1 ms/cm

STEP RESPONSE WITHOUT INPUT FILTER

FIGURE 20

STEP RESPONSE WITHOUT INPUT FILTER

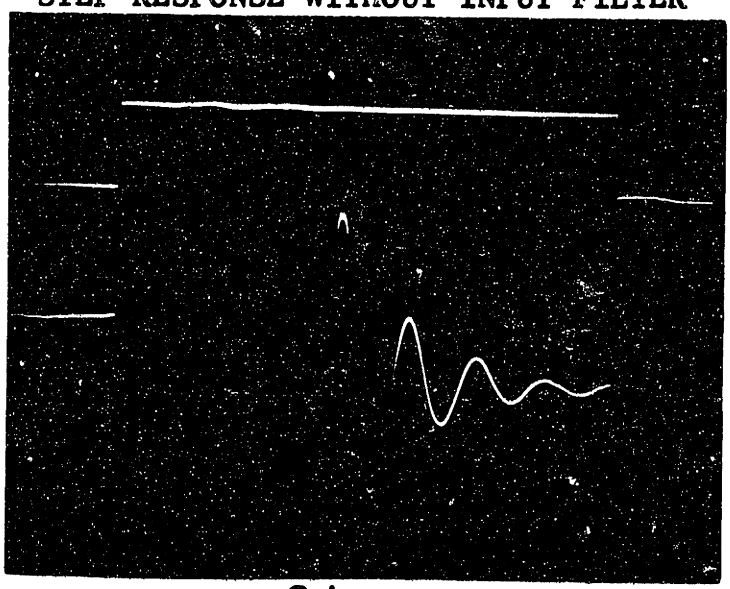

21

UPPER TRACE--STEP CHANGE IN e_c AT 0.2 VOLTS/CM
LOWER TRACE--RESPONSE OF e_p AT 0.2 VOLTS/CM
TIME SCALE--1 ms/cm

FIGURE 21

control voltage assuming $|P| = 2$. In Figures 20 and 21, e_c is centered about 3.75 volts where the measured magnitude of P is about 1.6. For this magnitude of P and G = 100 Equation 50 becomes:

$$e_p(t) = \frac{159c}{1.6} e^{-\sigma_o t} \left[\frac{\sigma_o}{\omega_o}\sin\omega_o t + \cos\omega_o t\right] u_{-1}(t) + \frac{c}{1.6} u_{-1}(t) \tag{59}$$

$$\sigma_o = 890 \text{ sec}^{-1}$$

$$f_o = \frac{\omega_o}{2\pi} = 1.2 \text{ KHz}$$

Equation 59 predicts an initial overshoot of 159 times the final value of $e_p(t)$ and a final value of 1/1.6 times the step change in control voltage. From Figure 20 we see that the initial overshot has been clipped by the oscillator, P, but it is much greater than 10 times the step change in control voltage. The measured value of f_o is about 870 Hz, and σ_o is approximately 785 sec^{-1}. The final value of $e_p(t)$ is measured as 1/1.3 times the step change in e_c from Figure 21.

Figure 22 shows the step response of $e_p(t)$ with the input filter added. By making the same changes in Equation 52 that were made in Equation 50, Equation 52 becomes:

$$e_p(t) = \frac{c}{1.6} u_{-1}(t) - \frac{c}{1.6} e^{-\sigma_o t} \left[\frac{\sigma_o}{\omega_o}\sin\omega_o t + \cos\omega_o t\right] u_{-1}(t) \tag{60}$$

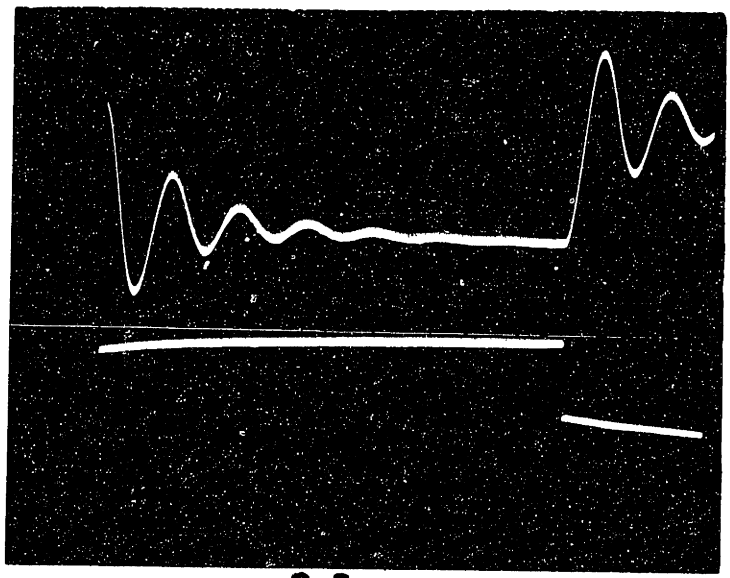

UPPER TRACE--RESPONSE OF e_p AT 0.1 VOLTS/CM
LOWER TRACE--STEP CHANGE IN e_c AT 0.2 VOLT/CM
TIME SCALE--1 ms/cm

STEP RESPONSE WITH INPUT FILTER ADDED

FIGURE 22

$$\sigma_o = 890$$

$$f_o = \frac{\omega_o}{2\pi} = 1.2 \text{ KHz}$$

Equation 60 indicates no initial overshoot in $e_p(t)$ and a peak overshoot of .7 times the final value. Figure 22 also shows zero initial overshoot and a peak overshoot of .5 times the final value. The value of f_o is measured as 870 Hz and σ_o is 452 sec^{-1} from Figure 22. Equation 60 indicates that the final value of $e_p(t)$ is 1/1.6 times the step change in e_c where as the measured value from Figure 22 is 1/1.2.

By comparing the measured step response with and without the input filter it can be seen that the input filter greatly reduces the peak overshoot and reduces the settling time of the system. These observations are in agreement with the theory presented in Chapter 2 on the step response of e_p.

4.4 Jitter in the Output Frequency

The peak error in the output frequency due to jitter is given by Equation 56 as 0.157% at f = 5MHz. Figure 23 shows this jitter as displayed on a sampling scope. The peak error in the period as measured from Figure 23 is about 0.15%. Since percentage frequency error is equivalent to

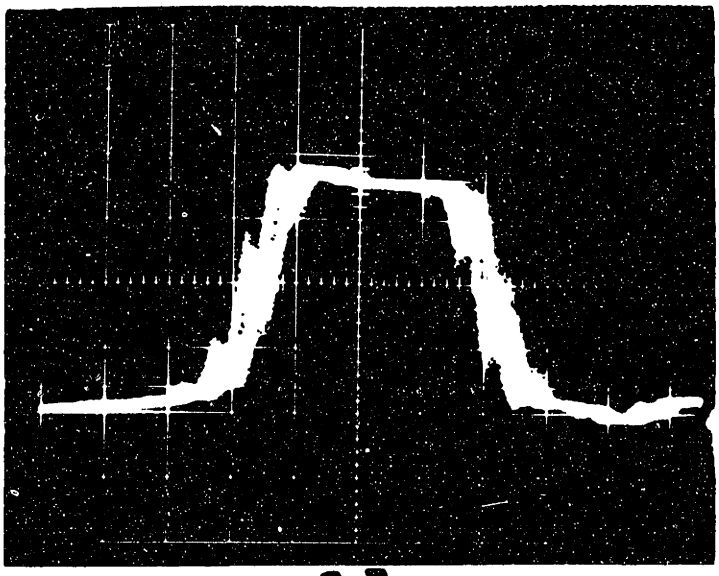

23

VERTICAL SCALE--100 mv/cm

TIME SCALE--1 ns/cm

JITTER AT 5 MHz

FIGURE 23

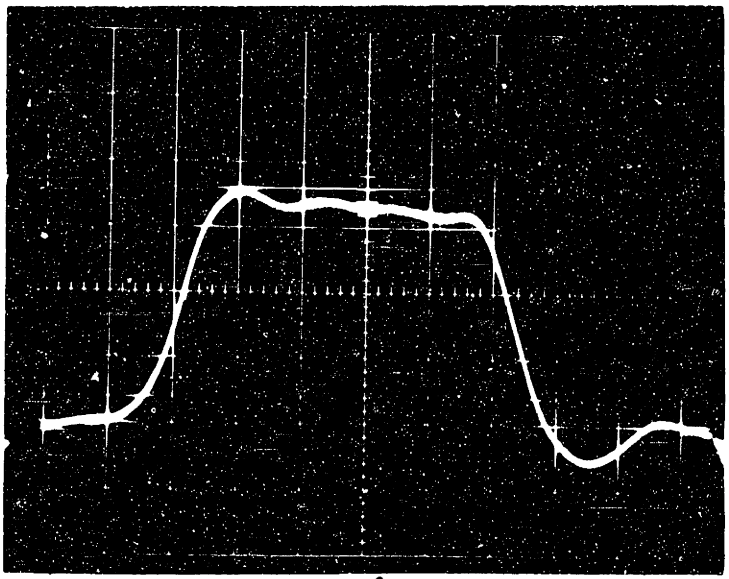

24

VERTICAL SCALE--100 mv/cm

TIME SCALE--1 ns/cm

JITTER AT 50 MHz

FIGURE 24

percentage period error when the error is small, the measured value compares favorably with the value in Equation 56.

Equation 55 indicates that the jitter goes as $1/f^2$ and therefore should not be noticeable at f = 50 MHz. By referring to Figure 24 we see that the jitter is considerably reduced at f = 50 MHz.

Figure 25 shows several cycles of the output waveform at 50 MHz.

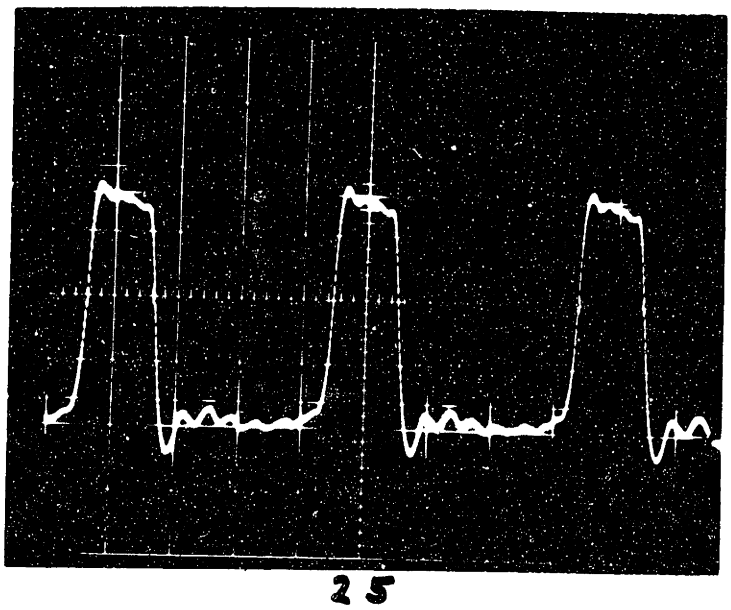

VERTICAL SCALE--100 mv/cm

TIME SCALE--5 ns/cm

OUTPUT WAVEFORM AT 50 MHz

FIGURE 25

5.0 SUMMARY AND CONCLUSIONS

The data presented in Chapter 4 shows that the final circuit was able to meet the design goals set forth in Chapter 1. The measured performance of the circuit also agreed well with the theoretical analysis of Chapter 2 indicating that this analysis represents an accurate model for the circuit.

One part of the system which needs improvement are the filters used in the feedback path and at the input. The step response is fairly slow, which in turn limits the bandwidth of this system as an F-M modulator. Perhaps some phase compensated filters could be designed which would allow a faster step response and still provide enough attenuation to limit the jitter in the output frequency.

Except for the filters, the circuit performed very satisfactorily and should require little further development for applications that are consistent with the design goals.

APPENDIX

A.1 Proof that $\delta_f(e_c) = -\delta_\ell(f)$

Suppose that the closed loop system is in the state e_c^*, f^* as shown in Figure 26.

$$\delta_f \triangleq \left(\frac{f^* - Ke_c^*}{Ke_c^*}\right) 100 = -\left(\frac{\Delta f}{Ke_c^*}\right) 100$$

$$\delta_\ell \triangleq \left(\frac{e_c^* - K^{-1}f^*}{K^{-1}f^*}\right) 100 = \left(\frac{\Delta e_c}{K^{-1}f^*}\right) 100$$

but $\frac{\Delta f}{\Delta e_c} = K$ from Figure 1A.

Therefore,

$$\delta_f = -\left(\frac{\Delta e_c K}{f^*}\right) 100 = -\left(\frac{\Delta e_c}{K^{-1}f^*}\right) 100 = -\delta_\ell$$

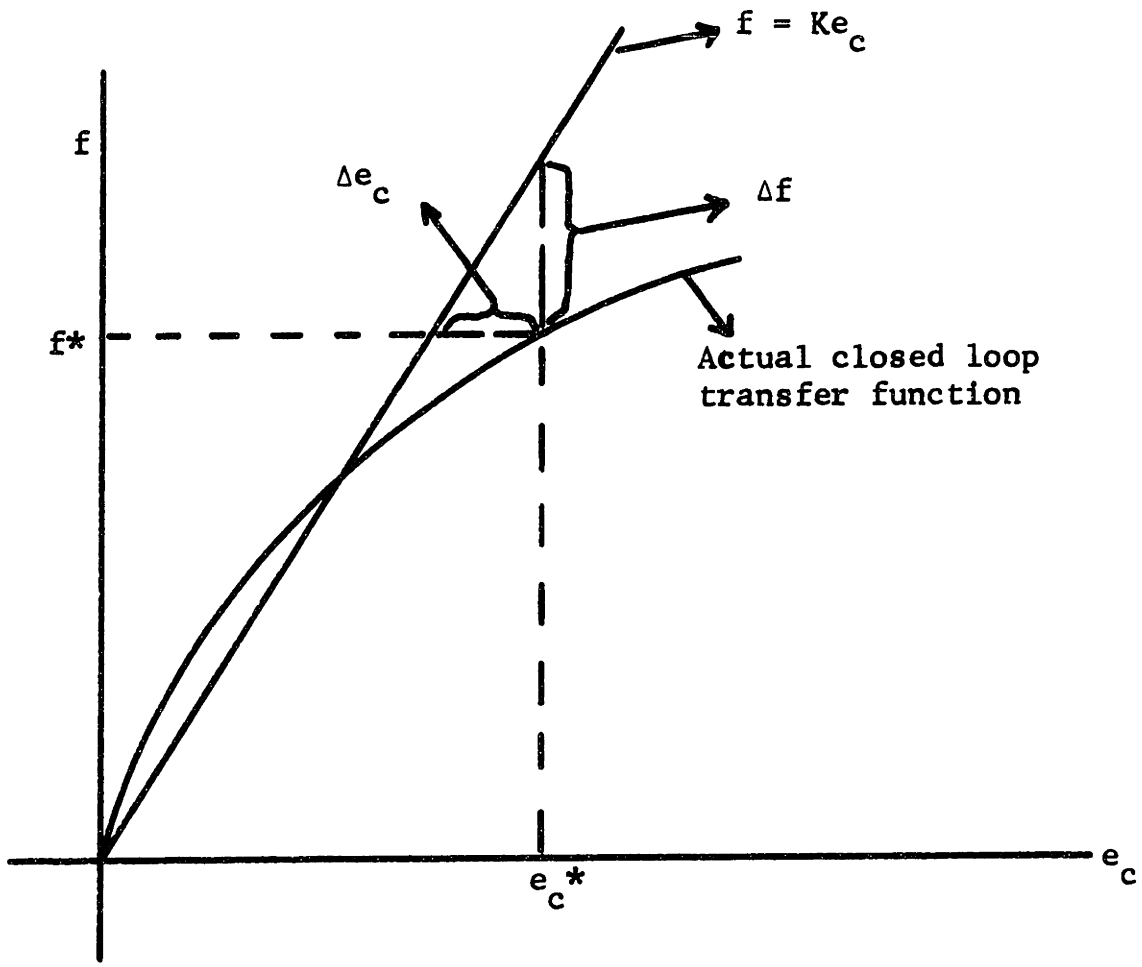

FIGURE 26

VOLTAGE CONTROL PULSE OS

FIGURE 27

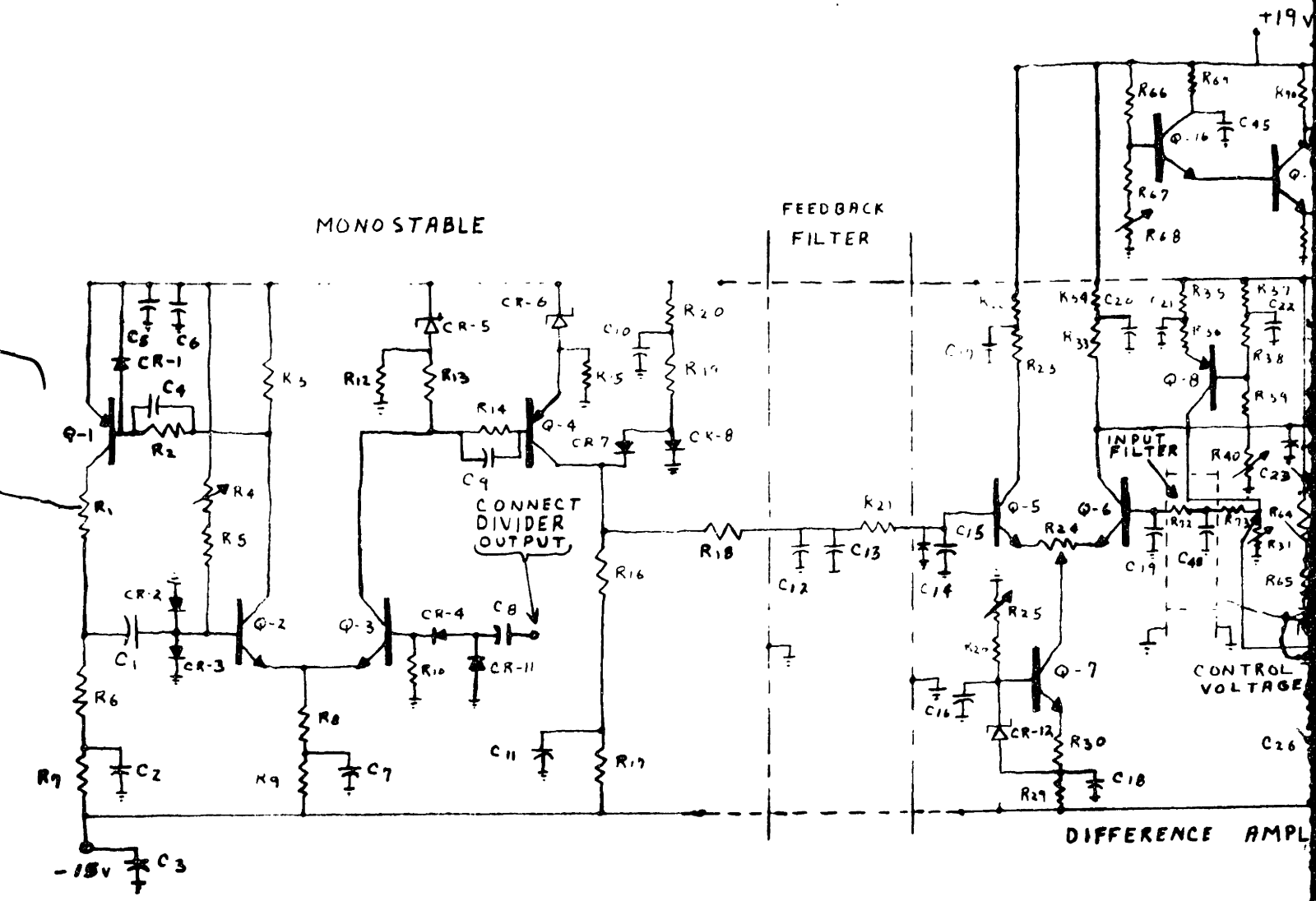

Q-17	2N 2218
Q-1	2N 2904
Q-2, Q-3, Q-7, Q-9, Q-10, Q-16	2N 3390
Q-4, Q-11	2N 3250
Q-5, Q-6	GR TR-46
Q-8	2N 3638
Q-12, Q-13	RCA
Q-14, Q-15	40237
CR-1, CR-2, CR-3, CR-4, CR-11	IN 3604
CR-5, CR-12	IN 752 SHARP
CR-6	IN 821-A
CR-7, CR-8	IN 4009
CR-9	IN 750

L_1, L_3	CHM-1 4.7 mh
L_2, L_4	CHM-8 .8 mh
C_1	COM-5F 525 pf
$C_2, C_7, C_{11}, C_{16}, C_{18}, C_{26}, C_{37}, C_{39}, C_6, C_{10}, C_{17}, C_{20}, C_{21}, C_{22}, C_{24}, C_{28}, C_{27}, C_{43}, C_{42}$	COE-60 3.3 mf

C_4, C_8, C_{29}	COM-2B 100 pf
C_8, C_{38}, C_{31}	
$C_{41}, C_{25}, C_{45}, C_{46}$	COC-61-3 .01 mf
C_9	COC-60 22 pf
C_{12}, C_{14}, C_{30}	COC-3 .001 mf
C_{13}, C_{15}, C_{23}	COP-24 .33 mf
	COC-60 47 pf
$C_{33}, C_{40}, C_{47}, C_{32}$	COF-60 1 mf
C_{34}	COC-1 2 pf
C_{36}	COC-1 1.8 pf
C_{35}	COT-29-2 3-12 pf
$C_6, C_{44}, C_{19}, C_{48}$	COE-89 33 mf

$R_1, R_{22}, R_{34}, R_{42}$	100 Ω
R_2	27 K
R_3, R_8	1.5 K
R_{19}, R_{64}	POSW-7
R_4, R_{50}	REF-90
R_5	REF-70
R_6	
$R_7, R_9, R_{17}, R_{29}, R_{53}$	
$R_{57}, R_{20}, R_{35}, R_{37}, R_{69}, R_{46}, R_{64}, R_{70}, R_{47}, R_{63}$	10 Ω
R_{10}	300 Ω
R_{25}	POSW-7
R_{12}, R_{15}	1.8 K
R_{13}, R_{52}, R_{26}	910 Ω
R_{14}	18 K

KB K

NTROL PULSE OSCILLATOR

FIGURE 27

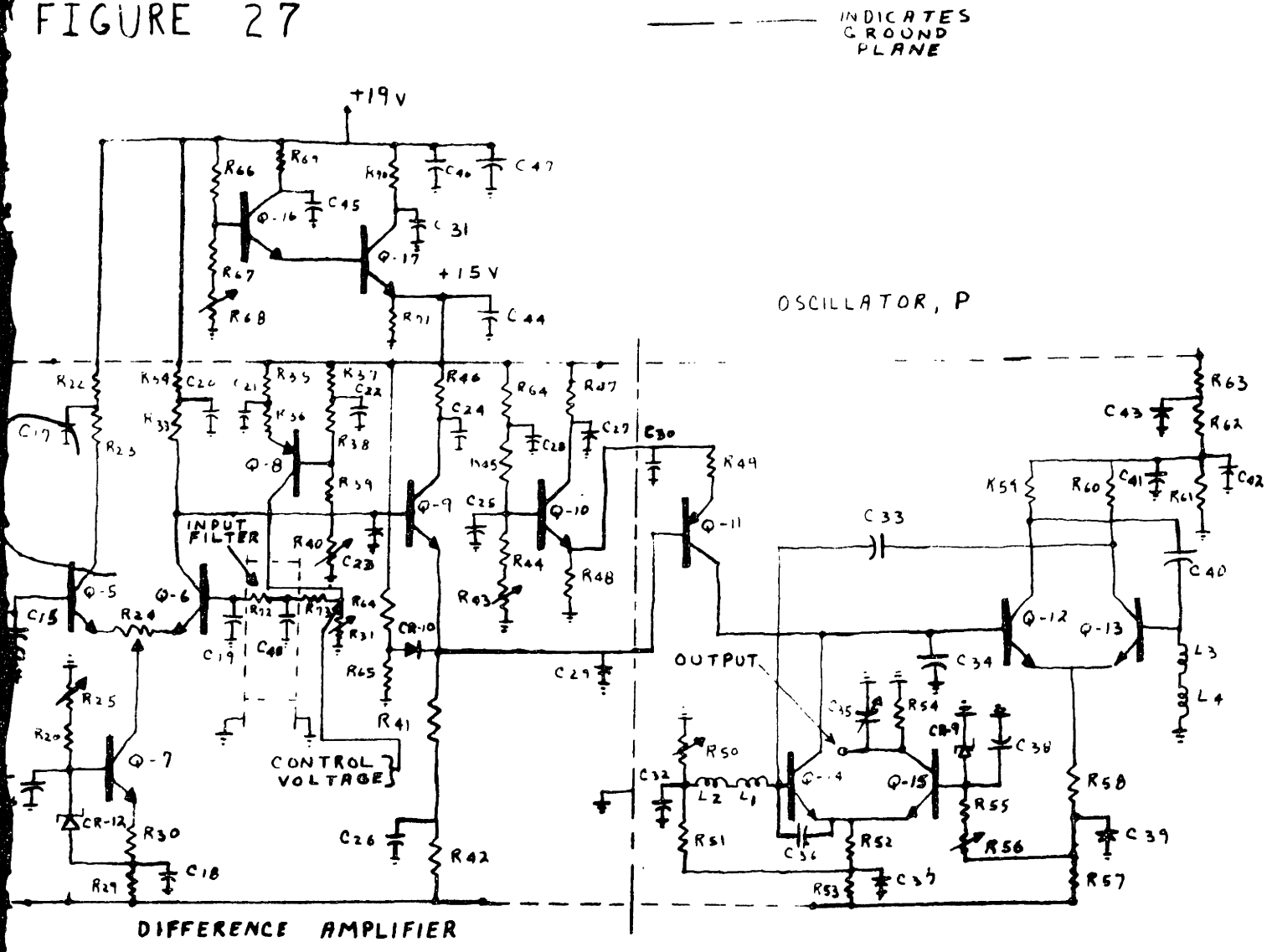

R1, R22	100 Ω	
R34, R42		
R2	27 K	
R3, R8	1.5 K	
R19, R64		
R4, R50	POSW-7	500 Ω
R5	REF-70	2740 Ω
R6	REF-70	2150 Ω
R7, R9		
R17, R29, R53		
R57, R20	10 Ω	
R35, R37, R69		
R46, R64, R70		
R47, R63		
R10	300 Ω	
R25	POSW-7	2 K
R12, R15	1.8 K	
R13, R52, R26	910 Ω	
R14	18 K	
R16	3 K	
R18, R21	5.1 K	
R23, R33	REF-70	34.0 K
R24	POSW-9	100 Ω
R40	POSW-9	1 K
R39	REF-70	11.0 K
R27, R38	REF-70	3400 Ω
R30	REF-70	12.7 K
R31	6-R/432-3	DECADE
R36	REF-70	2870 Ω
R41	2.2 K	
R45	REF-70	200 Ω
R44	REF-70	953
R43	POSW-9	200 Ω
R48	1.2 K	
R49	REF-70	1 K
R51	1 K	
R55, R58	1.1 K	
R56	POSW-7	2 K
R54	50 Ω (U56)	
R59	220 Ω	
R60	200 Ω	
R62	REF-70	226 Ω
R61	REF-70	536 Ω
R65	1.6 K	
R66	2.7 K	
R67	13 K	
R68	POSW-7	5 K
R71	15 K	
R72, R73	51 Ω	

REFERENCES

1. C. D. Clarke, "A Transistorized Voltage-Controlled Variable Pulse Rate Generator", Electronic Engineering, Vol. 34, No. 411, P. 322 (May 1962).

2. E. J. C. Fowell and A. Cowley, "A Voltage-Modulated Variable Pulse-Rate Generator", Electronic Engineering, Vol. 32, No. 387, P. 304-306, (May 1960).

3. J. J. Cooper, "A Wide Band Voltage Controlled Square Wave Generator with Linear Characteristics, "Electronic Engineering, Vol. 35, No. 427 (September 1963), P. 595-598.

4. Hewlett-Packard Co. Catalogue No. 25, P. 143.

5. Francis B. Hildebrand, "Advanced Calculus for Applications", Prentice-Hall, Inc., May 1963, P. 56, Eqn 15.

6. "IEEE International Convention Record", 1964, Vol. 12, Part 8, P. 129-136.